



HAL
open science

Aquatic carbon fluxes dampen the overall variation of net ecosystem productivity in the Amazon basin: An analysis of the interannual variability in the boundless carbon cycle

Adam Hastie, Ronny Lauerwald, Philippe Ciais, Pierre Régnier

► To cite this version:

Adam Hastie, Ronny Lauerwald, Philippe Ciais, Pierre Régnier. Aquatic carbon fluxes dampen the overall variation of net ecosystem productivity in the Amazon basin: An analysis of the interannual variability in the boundless carbon cycle. *Global Change Biology*, 2019, 25 (6), pp.2094-2111. <10.1111/gcb.14620>. <hal-02899755>

HAL Id: hal-02899755

<https://hal.science/hal-02899755v1>

Submitted on 16 Jun 2021

HAL is a multi-disciplinary open access archive for the deposit and dissemination of scientific research documents, whether they are published or not. The documents may come from teaching and research institutions in France or abroad, or from public or private research centers.

L'archive ouverte pluridisciplinaire **HAL**, est destinée au dépôt et à la diffusion de documents scientifiques de niveau recherche, publiés ou non, émanant des établissements d'enseignement et de recherche français ou étrangers, des laboratoires publics ou privés.



HAL Authorization



THE UNIVERSITY *of* EDINBURGH

Edinburgh Research Explorer

Aquatic carbon fluxes dampen the overall variation of net ecosystem productivity in the Amazon basin: An analysis of the interannual variability in the boundless carbon cycle

Citation for published version:

Hastie, A, Lauerwald, R, Ciais, P & Regnier, P 2019, 'Aquatic carbon fluxes dampen the overall variation of net ecosystem productivity in the Amazon basin: An analysis of the interannual variability in the boundless carbon cycle', *Global Change Biology*. <https://doi.org/10.1111/gcb.14620>

Digital Object Identifier (DOI):

[10.1111/gcb.14620](https://doi.org/10.1111/gcb.14620)

Link:

[Link to publication record in Edinburgh Research Explorer](#)

Document Version:

Peer reviewed version

Published In:

Global Change Biology

General rights

Copyright for the publications made accessible via the Edinburgh Research Explorer is retained by the author(s) and / or other copyright owners and it is a condition of accessing these publications that users recognise and abide by the legal requirements associated with these rights.

Take down policy

The University of Edinburgh has made every reasonable effort to ensure that Edinburgh Research Explorer content complies with UK legislation. If you believe that the public display of this file breaches copyright please contact openaccess@ed.ac.uk providing details, and we will remove access to the work immediately and investigate your claim.



1 **Aquatic carbon fluxes dampen the overall variation of net ecosystem**
2 **productivity in the Amazon basin: An analysis of the interannual**
3 **variability in the boundless carbon cycle.**

4 Adam Hastie¹ | Ronny Lauerwald^{1,2} | Philippe Ciais³

5 | Pierre Regnier¹

6 ¹Biogeochemistry and Earth System Modelling, Department of Geoscience, Environment and Society,
7 Universite Libre de Bruxelles, Bruxelles, Belgium

8 ²College of Engineering, Mathematics and Physical Sciences, University of Exeter, Exeter, UK

9 ³Laboratoire des Sciences du Climat et de l'Environnement, UMR8212, CEA-CNRS-UVSQ F-91191
10 Gif sur Yvette, France

11
12 **Abstract**

13 The river-floodplain network plays an important role in the carbon (C) budget of the Amazon
14 basin, as it transports and processes a significant fraction of the C fixed by terrestrial
15 vegetation, most of which evades as CO₂ from rivers and floodplains back to the atmosphere.
16 There is empirical evidence that exceptionally dry or wet years have an impact on the net C
17 balance in the Amazon. While seasonal and interannual variations in hydrology have a direct
18 impact on the amounts of C transferred through the river-floodplain system, it is not known
19 how far the variation of these fluxes affects the overall Amazon C budget.

20 Here, we introduce a new wetland forcing file for the ORCHILEAK model, which improves
21 the representation of floodplain dynamics and allows us to closely reproduce data-driven
22 estimates of net C exports through the river-floodplain network. Based on this new wetland
23 forcing and two climate forcing datasets, we show that across the Amazon, the percentage of
24 NPP lost to the river-floodplain system is highly variable at the interannual timescale and wet
25 years fuel aquatic CO₂ evasion. However, at the same time overall net ecosystem productivity
26 (NEP) and C sequestration is highest during wet years, partly due to reduced decomposition
27 rates in water-logged floodplain soils. It is years with the lowest discharge and floodplain
28 inundation, often associated with El Nino events, that have the lowest NEP and the highest
29 total (terrestrial plus aquatic) CO₂ emissions back to atmosphere. Furthermore, we find that
30 aquatic C fluxes display greater variation than terrestrial C fluxes, and that this variation
31 significantly dampens the interannual variability in NEP of the Amazon basin. These results

32 call for a more integrative view of the C fluxes through the vegetation-soil-river-floodplain
33 continuum, which directly places aquatic C fluxes into the overall C budget of the Amazon
34 basin.

35

36 1. Introduction

37 The land-ocean aquatic continuum (LOAC) is now well established as an important
38 component of the global carbon (C) cycle (Ciais et al., 2013). Atmospheric C fixed in
39 terrestrial ecosystems and wetlands can be lost through respiration, and stored in biomass and
40 soil, but can also be transferred laterally to the LOAC as dissolved organic carbon (DOC),
41 particulate organic carbon (POC) and dissolved CO₂. Along the LOAC this C can in turn
42 undergo biogeochemical transformations, be lost back to the atmosphere via CO₂ evasion,
43 transferred further downstream to estuaries and the coast, or undergo sedimentation in
44 wetlands (incl. lakes and reservoirs). It has been demonstrated at the catchment (Cole &
45 Caraco, 2001) to global scale (Battin et al., 2009; Regnier et al., 2013; Ciais et al. in review),
46 that these fluxes are important and should not be neglected in land C budgets.

47 Globally, there remains a high degree of uncertainty associated with the amounts of C being
48 transferred through and processed within the LOAC. Estimates of the total amount of
49 terrestrial C inputs to inland waters range widely from 1.1 to 5.1 Pg C yr⁻¹ (Cole et al., 2007;
50 Aufdenkampe et al., 2011; Regnier et al., 2013; Drake et al., 2017), reflecting the fact that
51 this flux is indirectly derived by summing estimates of aquatic CO₂ evasion, C exports to the
52 coast and burial in the LOAC. Of the three constituent fluxes, CO₂ evasion is the largest
53 (Drake et al., 2017) and thus uncertainties in CO₂ evasion dominate the subsequent
54 uncertainty in the export of terrestrial C to inland waters. Moreover, aquatic CO₂ evasion is
55 highly spatially variable and hotspot regions have been identified; the boreal and tropical

56 regions contributing disproportionately to global CO₂ evasion from lakes (Hastie et al., 2018)
57 and rivers (Lauerwald et al., 2015), respectively.

58 In the Tropics, high terrestrial net primary productivity (NPP) and high rainfall drive a large
59 export of C to inland waters and in turn high aquatic CO₂ evasion. In 2002, Richey et al.
60 extrapolated observed *p*CO₂ measurements to estimate a total CO₂ evasion flux of 0.47 Pg C
61 yr⁻¹ from the inland waters of the Amazon Basin (upstream of Obidos, see Fig. S1), 13 times
62 greater than their 36 Tg C yr⁻¹ estimate of the total organic C (TOC) export to the coast. In
63 2013, Rasera et al. calculated a substantially higher CO₂ evasion of 0.8 Pg C yr⁻¹ over the
64 same basin area, largely as a result of higher values of gas exchange velocity (*K*₆₀₀). More
65 recently, Sawakuchi et al. (2017) added observations from the basin area downstream of
66 Obidos and concluded that CO₂ evasion from the entire Amazon Basin (down to mouth)
67 could potentially be as high as 1.39 Pg C yr⁻¹.

68 Previous studies have shown that there is considerable seasonal variation in aquatic CO₂
69 evasion. Richey et al. (2002), found that the partial pressure of CO₂ (*p*CO₂) and in turn CO₂
70 evasion was tightly coupled to discharge, increasing and decreasing with rising and falling
71 water respectively. Moreover, they measured exceptionally high *p*CO₂ values (>44,000 μatm)
72 on the floodplain of the mainstem of the Amazon, and speculated that the source of the C is
73 likely to be organic matter exported from flooded forests.

74 This was later confirmed by Abril et al. (2014) who demonstrated that Amazonian wetlands
75 export around 50% of their GPP to inland waters in contrast to the typical values of <2%
76 exported from terrestrial landscapes. They went on to conclude that the lateral C flux from
77 wetlands is enough to account for around 210 Tg C yr⁻¹ of the total CO₂ evasion flux from the
78 inland waters of the Amazon river-floodplain network. A recent study by Almeida et al
79 (2017) demonstrated that in addition to seasonal variation, large flood events also drive

80 interannual variation in CO₂ evasion from the Madeira River (a tributary of the Amazon),
81 namely that years with extreme flooding evade 20% more CO₂ to the atmosphere per unit
82 area than years without. Another flux linked to flood events is C burial and a recent study
83 estimated the POC burial flux in Amazon floodplain lakes at 16 Tg C yr⁻¹ (Sanders et al.,
84 2017), at least an order of magnitude lower than estimates of CO₂ evasion.

85 These observed seasonal and interannual signals in C fluxes are particularly important given
86 that the region is increasingly vulnerable to extreme climatic events such as droughts and
87 floods (Marengo et al., 2011; Chou et al., 2013; Gloor et al., 2013; Zulkafli et al., 2016).

88 Indeed, recent studies have shown substantial decreases in terrestrial net primary productivity
89 (NPP), and in turn C uptake from the atmosphere as a result of the 2005 and 2010 droughts
90 (Zhao & Running, 2010; Potter et al., 2011; Gatti et al., 2014; Doughty et al., 2015 and
91 Feldpausch et al., 2016). However, most of these studies do not account for LOAC fluxes.

92 For these reasons, it is important that we understand the interannual variation in LOAC fluxes
93 and how they influence the overall net ecosystem production (NEP) of the entire Amazon
94 Basin.

95 With this in mind, we aim to tackle the following research questions:

- 96 • To what extent do the LOAC fluxes (aquatic CO₂ evasion and C export to the coast)
97 vary inter-annually and seasonally throughout the entire Amazon Basin?
- 98 • How does interannual variation in discharge and flooding affect the LOAC fluxes,
99 terrestrial NPP, soil heterotrophic respiration (SHR) and ultimately the NEP of the
100 Amazon Basin, particularly in the context of increasing climatic extremes? More
101 specifically, does the incorporation of LOAC fluxes amplify or dampen variation in
102 NEP?

103 Upscaling studies and empirical models are useful in providing estimates of individual
104 components of the LOAC fluxes for the present day. However, these methods cannot
105 represent the interaction between the different aspects of the Amazon Basin C cycle. A more
106 complex and integrated modelling approach is required to understand and, ultimately, predict
107 the longer-term variation in LOAC fluxes and how this variation affects the net C balance of
108 these ecosystems.

109 In 2017, Lauerwald et al. developed the first full Land Surface Model (ORCHILEAK model)
110 approach to represent the lateral C fluxes along the LOAC in the Amazon Basin and similarly
111 demonstrated the significance of wetlands, concluding that 51% of total CO₂ evasion comes
112 from the floodplains. The study estimated a total CO₂ evasion of 379 C Tg yr⁻¹, close to the
113 value produced by Richey et al. from up-scaling of measurements. In addition, they
114 substantiated the idea that wetlands are a disproportionately important source of C to rivers,
115 calculating that the CO₂ inputs from root and heterotrophic respiration in flooded soils are
116 almost twice that from non-flooded soils.

117 The land surface model approach undertaken by Lauerwald et al. (2017) provides a valuable
118 tool for further research, in particular the capability to make future projections of the LOAC
119 C fluxes. However, while they were able to reproduce the seasonality in discharge on the
120 main stem of the Amazon, the total flooded area was substantially underestimated when
121 compared to the observed data of Richey et al., 2013 (after Hess et al., 2003). This is because
122 Lauerwald et al. (2017) relied on the coarse (0.25°) global inundation dataset of Prigent et al.
123 (2007), which tends to underestimate the total floodable area (Lauerwald et al., 2017). Given
124 previous estimates of the magnitude of the CO₂ evasion flux from the Amazon floodplain, the
125 importance of wetlands, and the region's increasing vulnerability to climatic extremes; it is
126 vital that we can accurately model its floodplain dynamics.

127 In this study, an improved representation of floodplain and wetland dynamics is achieved
128 through the production of a new floodplain forcing file for the ORCHILEAK model, from the
129 high resolution (100m or 0.0008°) synthetic aperture radar (SAR) dataset of Hess et al.
130 (2015). We use this new forcing file to improve the simulation of the interannual variation of
131 LOAC fluxes. In turn, we are able to address the research questions previously outlined, and
132 more specifically to evaluate the impact of flood extent on the dynamics of LOAC fluxes, and
133 ultimately how interannual variation in these aquatic C fluxes influences the overall variation
134 in NEP in the Amazon.

135

136 2. Methods

137 2.1 A brief description of the ORCHILEAK land surface model

138 ORCHILEAK (Lauerwald et al., 2017) is a new model branch of ORCHIDEE (Organizing
139 Carbon and Hydrology in Dynamic Ecosystems) (Krinner et al. 2005), the land surface
140 component of the Institut Pierre-Simon Laplace (IPSL) earth system model (ESM). It
141 simulates the production of DOC in the canopy and soils, the leaching of DOC and CO₂ from
142 soils to the river network, DOC mineralization and the subsequent CO₂ evasion from the
143 water surface. Crucially, it also simulates the exchange of C between litter, soils and water on
144 floodplains and in swamps. The representation of these fluxes is in turn closely coupled to the
145 hydrology scheme, namely the representation of precipitation, throughfall, surface runoff,
146 drainage, and the routing of discharge along the river-floodplain network. At the same time,
147 ORCHILEAK also simulates vegetation dynamics of 12 plant functional types, 5 of which
148 are present in the Amazon, as well as the C balance of biomass, litter and soils. In short,
149 ORCHILEAK integrates LOAC fluxes within a full representation of the terrestrial C cycling
150 as simulated by ORCHIDEE. However, in its current form ORCHILEAK does not account

151 for the burial of POC in fluvial and floodplain sediments or the evasion of C to the
152 atmosphere as CH₄. These fluxes are further discussed later. While the model does not
153 simulate the lateral transport of POC, it does account for the decomposition of submerged
154 litter as a substantial source of DOC and dissolved CO₂ to the water column; in other words,
155 POC from submerged litter is assumed to decompose locally in ORCHILEAK. The model is
156 described in more detail in the proceeding sections. For a full model description, as well as a
157 discussion on model assumptions and limitations, please refer to Lauerwald et al. (2017).

158 2.2 Overview of the hydrology, soil C scheme, and the transport and transformation of 159 aquatic C fluxes in ORCHILEAK

160 Precipitation and other meteorological input parameters are prescribed by a forcing file. The
161 hydrology module of ORCHILEAK, just like that of the standard version of ORCHIDEE,
162 partitions the precipitation between interception loss in the vegetation canopy and throughfall
163 to the ground. The throughfall is further partitioned into infiltration and surface runoff. The
164 soil water storage is refilled by infiltration and depleted by evapotranspiration and drainage.
165 The soil hydrology is represented using a 2 m soil column vertically discretized into 11 layers
166 of geometrically increasing thickness from top to bottom. These processes are all represented
167 at a 30 min time step (see d'Orgeval et al., 2008, Rosnay et al., 2002 for details).

168 ORCHILEAK incorporates a soil C module largely based on ORCHIDEE-SOM (Camino-
169 Serrano, 2018). The soil module uses the hydrological module outputs to simulate microbial
170 production and consumption of DOC, sorption and desorption of DOC on soil organic matter,
171 the advection and diffusion of DOC and dissolved CO₂ within the soil column and their
172 subsequent lateral export via runoff and drainage as well as the throughfall of DOC onto the
173 soil or water surface. There are 3 pools of DOC in the soil which are defined by their source
174 material and residence times (τ_{carbon}); the active, slow and passive pool. ORCHILEAK

175 distinguishes between flooded and non-flooded soils; decomposition rates of litter, SOC and
176 DOC being 3 times lower in flooded soils. Furthermore, it simulates the input of C to the
177 water column from flooded soils; DOC from litter and SOC decomposition from the top 4.5
178 cm of the soil column feeds directly to the DOC pool of the overlying waterbody.

179 The river routing module of ORCHILEAK routes the runoff and drainage from the hydrology
180 module and the corresponding dissolved C fluxes from the soil C module as river flow at a
181 daily time-step along a gridded river routing scheme at 0.5° resolution (Vorosmarty et al.,
182 2000). The river network is connected to two sorts of wetland, floodplains and swamps.

183 Where a swamp is present, a constant fraction of the river flow is feeding into the bottom of
184 the soil column. Where a floodplain is present, a temporary water body of time-variant
185 surface and volume may be formed beside the river channel and it is fed by a fraction of river
186 flow when bank-full discharge is surpassed. In the case of the Amazon basin, the bankfull
187 discharge threshold was defined as the median discharge simulated over the period 1980-
188 2000 (see Lauerwald et al., 2017). From the inundated floodplain, water and dissolved C may
189 infiltrate back into the soil or flow back into the river channel, while water may also
190 evaporate. The maximal floodable area (MFF) and the areal fraction of swamps (MFS) per
191 simulation grid is prescribed by a forcing file. The water that infiltrates back into the soil is
192 returned to the hydrology module. The dissolved C contained in that water is returned to the
193 soil C module.

194 ORCHILEAK simulates the transport and decomposition of terrestrial C inputs within the
195 routing scheme, with the assumption that the lateral transport of DOC and CO₂ are
196 proportional to discharge. Within the water column, DOC is separated into a labile and
197 refractory pool, with half-life times of 2 and 80 days, respectively. The labile pool
198 corresponds to the active pool of the soil C scheme, while the refractory pool is derived from
199 the slow and passive soil solution DOC pools combined. In order to ensure numerical

200 precision, CO₂ production and evasion from the water column, as well CO₂ inputs from
201 flooded litter and SOC are simulated at the high temporal resolution of 1/240 day (6 min).
202 *p*CO₂ is calculated at the same 6 min time-step based on the dissolved CO₂ concentration, and
203 the temperature-dependent solubility of CO₂. *p*CO₂ is then used along with a gas exchange
204 velocity and a diurnally variable water surface area, to calculate CO₂ evasion. Fixed gas
205 exchange values of 3.5 m d⁻¹ and 0.65 m d⁻¹ are used for rivers (and open floodplains) and
206 forested floodplains, respectively. Flooded forests are given a lower gas exchange velocity
207 due to the reduced impact of wind (i.e. lower wind speeds). For a more detailed explanation,
208 see Lauerwald et al. (2017).

209 2.3 New wetland forcing files

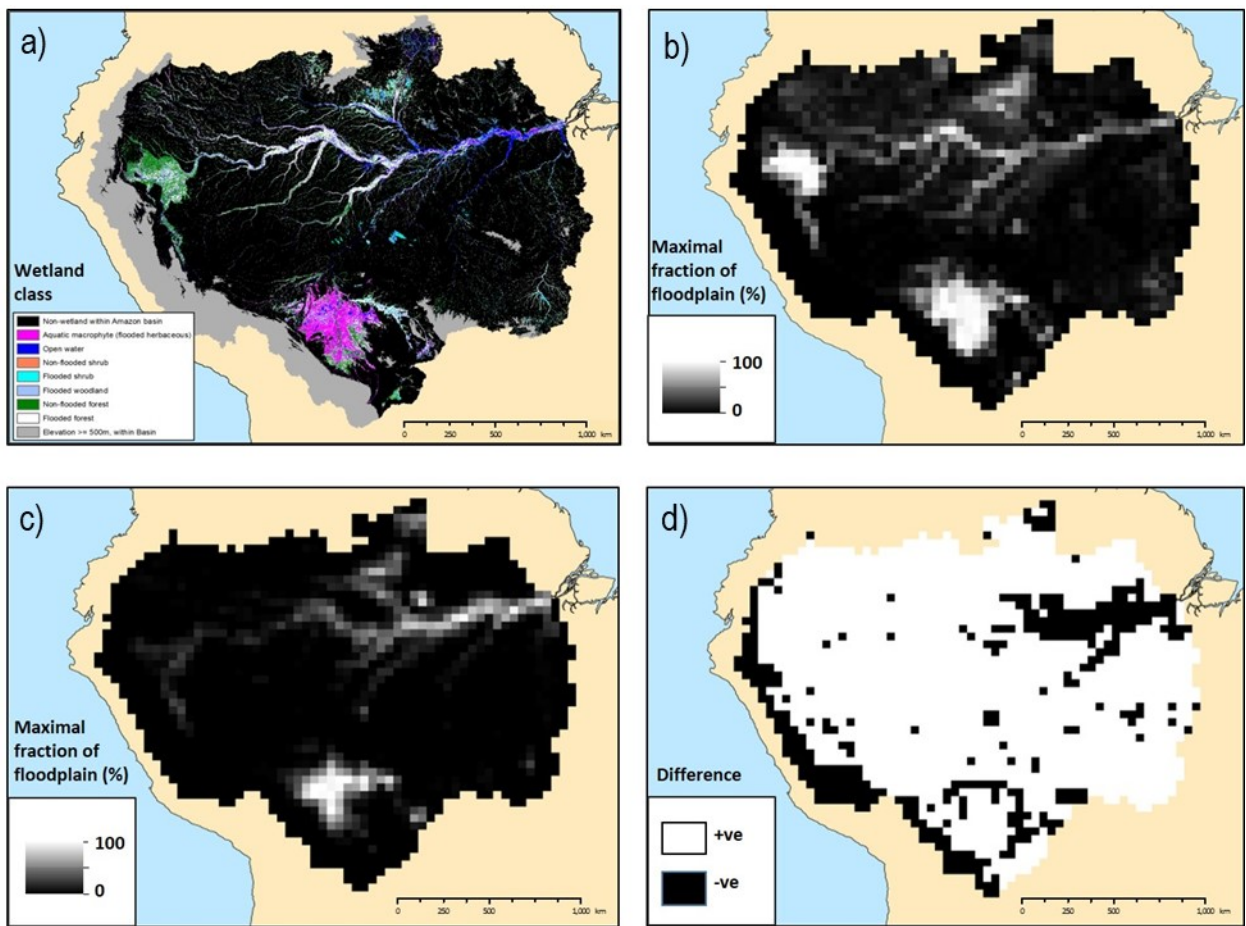
210 The original routing scheme of ORCHIDEE used universal MFF and MFS derived from the
211 Global Lakes and Wetlands Database (GLWD, Lehner and Doll, 2004) that were shown to
212 considerably underestimate inundated areas in the Amazon (Guimberteau et al., 2012). As a
213 result, Guimberteau et al. developed new MFF and MFS based on the 0.25° datasets of
214 Prigent et al. (2007) and Martinez and Le Toan (2007), respectively. This led to some
215 improvement but inundation was still substantially underestimated in the Amazon Basin.

216 In the Guimberteau datasets, “swamps”, defined as the vegetated part of maximum
217 floodplain, were subtracted from the MFF and used to create the separate swamp (MFS)
218 forcing file. In ORCHILEAK (Lauerwald et al., 2017), swamps were reincorporated into the
219 MFF forcing file, creating a larger, more realistic MFF, and representing the total flooded
220 area from which inland water CO₂ is evading. While these modifications again led to some
221 improvement in the representation of floodplains and swamps in ORCHILEAK, it
222 fundamentally still relied on a low resolution (0.25°) dataset, missing smaller areas of

223 inundation, and meaning that the overall maximum floodplain extent was too small
224 (Lauerwald et al., 2017).

225 With these limitations in mind, we created a new maximal fraction of floodplain (MFF,
226 Fig.1) forcing file for the ORCHILEAK model based on the 100m Synthetic Aperture Radar
227 (SAR) data described in Hess et al. (2015, see Fig.1 a). This dataset represents different
228 wetland types during the 1996 May-June flood season. Firstly, we merged all of the wetland
229 categories in Fig. 1 a) into one class, with the exception of the ‘non-wetland within the
230 Amazon Basin’, ‘Open water’ and ‘Elevation \geq 500 m, in Basin’ categories. We then
231 aggregated the merged dataset to a resolution of 0.5° (Fig.1 b). Note that in the MFF we
232 included three classes of land cover that were not flooded during the 1996 flood season,
233 namely ‘non-flooded shrubs’, ‘non-flooded woodlands’ and ‘non-flooded forest’ (classes 44,
234 66 and 88). This decision is based on the justification provided in Hess et al. that these “areas
235 not flooded on either date, but adjacent to flooded areas and displaying landforms consistent
236 with wetland geomorphology”. In other words, while these areas were not flooded in 1996,
237 they are likely prone to inundation in other years with greater precipitation and thus should be
238 included in maximum flood extent. Across the Amazon basin, the new forcing file prescribes
239 an average MFF of 13.6%, approximately twofold greater than the 6.3% produced with the
240 original ORCHILEAK forcing derived from Prigent et al. (2007) (Fig. 1 c, d). The addition
241 of the 44, 66 and 88 land cover classes makes a moderate difference; we produce an average
242 MFF of 10% without these 3 classes. For comparison, we also aggregated the 232m
243 resolution wetland dataset of Gumbricht et al. (2017). Assuming that all of the wetland
244 categories in Gumbricht et al. (2017) contribute to the maximum flood extent, we produce an
245 average MFF of 14.9%. However, we chose to use the MFF derived from Hess et al. (2015)
246 as it is measured at a higher resolution and considers wetlands as synonymous with
247 floodplains, while Gumbricht et al. (2017) has a wider definition. In order to account for the

248 uncertainty associated with the MFF forcing file we created two new versions of it; one in
 249 which the MFF of each grid was systematically increased by 7% (excluding “highland” areas
 250 $\geq 500\text{m}$ identified in Hess et al., 2015) (MFF+7), and another where the MFF was decreased
 251 by 7% (MFF-7). We chose a value of 7% as this is the inferred error of the original dataset,
 252 described in Hess et al. (2015). Across the Amazon basin, the MFF-7 forcing gives an
 253 average MFF of 9.3% while the MFF+7 gives an average of 18.3%. This range also envelops
 254 the uncertainty associated with the inclusion or exclusion of classes 44, 66 and 88, as well as
 255 that associated with the difference between the Hess and Gumbrecht datasets.

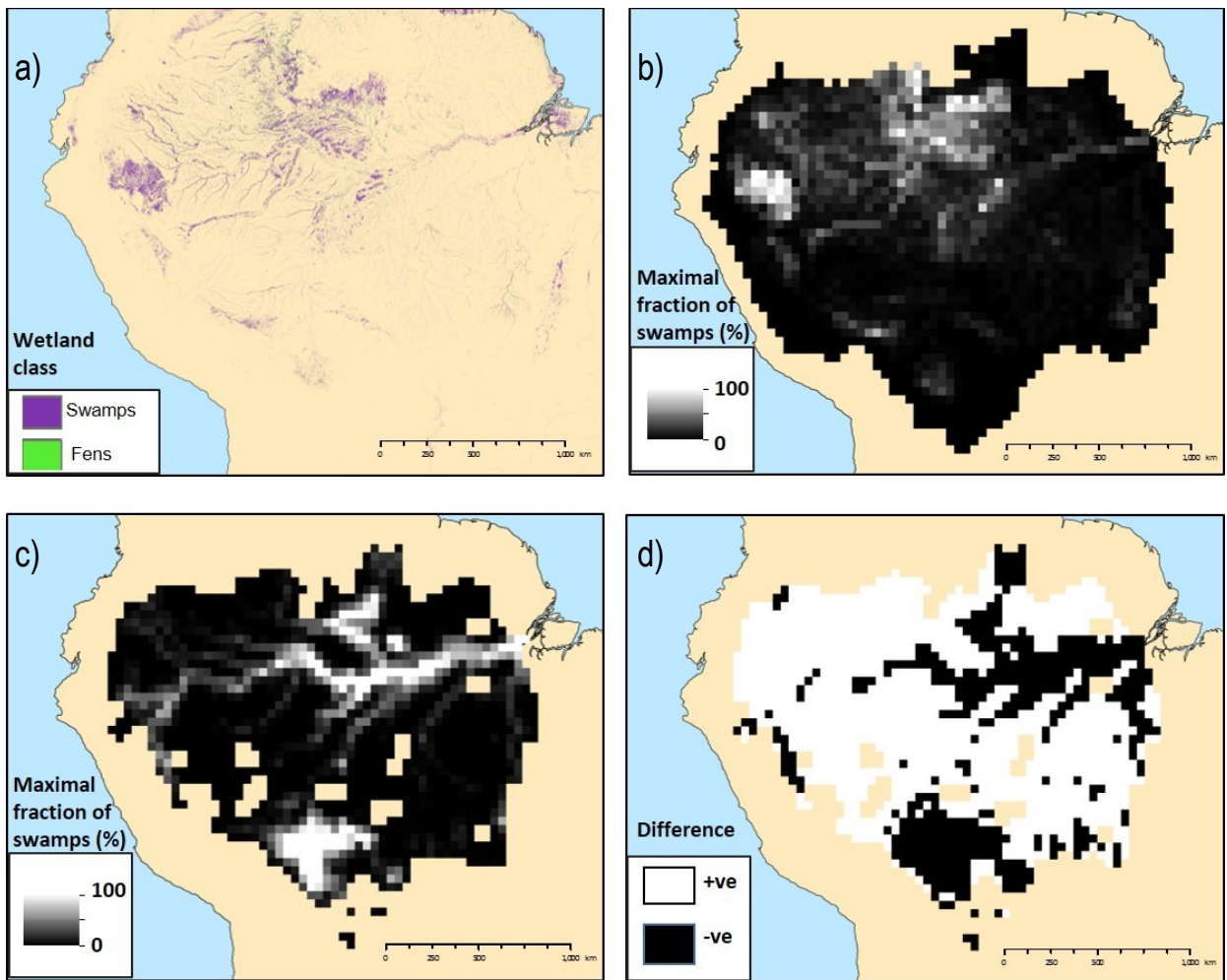


256
 257 Figure 1. a) Wetland classification within the Amazon Basin (Hess et al., 2015), b); the new
 258 maximal fraction of floodplain (MFF) forcing file derived from Hess et al. (2015) data, c) the
 259 previous MFF forcing file (Guimberteau et al., 2012) and d) the difference between the new
 260 and old MFF. In pane d), “+ve” refers to an increase in MFF with the new MF forcing, while
 261 “-ve” refers to a decrease. Maps in panels b-d are at a resolution of 0.5° .

262

263 We also created a new ORCHILEAK maximal fraction of swamps (MFS, Fig. 2) forcing file
264 based on the 232 m resolution tropical wetland dataset of Gumbricht et al (2017), as the Hess
265 et al. (2015) dataset does not define an explicit “swamp” category. We extracted class 30
266 (Swamps incl. bogs) and 40 (Fens), before merging these classes and aggregating them to the
267 0.5° resolution. Across the Amazon basin, the new forcing file prescribes an average MFS of
268 5.4% (Fig.2, b) which is comparable to the 6% produced with the previous approach
269 (Guimberteau et al., 2012) (Fig. 2, c, d).

270
271



272

273 Figure 2. a) Swamps and ferns classification within Amazon Basin from Gumbricht et al
274 (2017) b); the new maximal fraction of swamps (MFS) forcing file derived from Gumbricht
275 et al. (2017) data, c); the previous MFS forcing file (Lauerwald et al., 2017) and d) the

276 difference between the new and old MFS. In pane d), “+ve” refers to an increase in MFF with
277 the new MF forcing, while “-ve” refers to a decrease. Maps in panels b-d are at a resolution
278 of 0.5°.

279

280 2.4 Simulation Set-up

281 Model configuration

282 The model was initially run from 1980 until 2000 using two different climate forcing
283 datasets, namely Princeton GPCP (Sheffield et al., 2006), and a regionally updated version of
284 NCC (Ngo-Duc et al., 2005) which was introduced by Guimberteau et al. (2012). This was
285 done in order to test which dataset is able to better recreate observed discharge and the
286 associated seasonal and interannual variability in floodplain inundation, as well as to account
287 for the uncertainty associated with choice of climate forcing. With the combination of the two
288 climate forcing files and the three MFF forcing files, we ran six different model
289 configurations. Model parameterisation can also cause uncertainty such as the setting of
290 decomposition rate constants for labile and refractory DOC within ORCHILEAK. However,
291 the impact of these parameters was already investigated via a sensitivity analyses in the paper
292 describing the development of the ORCHILEAK model (Lauerwald et al., 2017). As such,
293 we chose to focus on climate forcing and floodplain area as sources of uncertainty in
294 combination with substantial validation against observations and model outputs from the
295 literature.

296 The original ORCHILEAK simulation (Lauerwald et al., 2017) used only the updated NCC
297 climate forcing. Here, we ran four simulations with the NCC climate forcing dataset; one
298 with the new versions of MFF (hereafter referred to as “standard MFF”) and MFS, two more
299 to account for the uncertainty in MFF (MFF+7 & MFF-7), and another with the old MFF
300 (Lauerwald et al., 2017), in order to determine the impact of the new wetland forcing files.

301 We ran the Princeton GPCC simulations with the new versions of MFF and MFS only (three
302 runs). Model parameterisation follows Lauerwald et al. (2017).

303 Hydrology statistics

304 Following Lauerwald et al. (2017), we calculated a series of statistical parameters in order to
305 calibrate the flood dynamics of the model in a robust and consistent manner. After an initial
306 run, we calculated bank-full discharge and the median water storage for each grid cell (1980-
307 2000), for each model configuration. Any discharge in excess of the median water storage
308 will overtop and begin to inundate the floodplains. After updating bank-full discharge and re-
309 running each model configuration, we calculated the 95th percentile of all simulated water
310 level heights (1980-2000) for each grid cell. This represents the maximum water level, at
311 which the maximum floodable area is inundated. Once this was updated, each model
312 configuration was re-run once more.

313 Soil carbon spin up

314 In order to reach a steady state soil carbon pool, we spun-up the model for a total of
315 approximately 7,000 years, looping over 10 years of climate forcing data (1948-1957). To
316 reach steady state more quickly, we first ran the model for 2000 years with the default soil
317 carbon residence time (τ_{carbon}) values halved and a constant atmospheric CO₂ concentration of
318 350 μatm . Land-cover, representative of the first year of climate forcing data (1948),
319 remained constant over these spin-up runs. After this procedure, all of the soil C pools were
320 approximately at steady state (<0.01% change over the last century of the spin up). Note that
321 it is assumed that soil C pools were in quasi steady state before significant human impact.

322 Transient simulations

323 We then performed a transient (industrial) run from 1860, until the year that the particular
324 climate forcing dataset starts from (for example to 1948 for Princeton GPCC), again looping

325 over 10 years of climate data but with transient land-cover (LUH-CMIP5) and atmospheric
326 CO₂. Finally, we performed a fully transient simulation (land-cover, atmospheric CO₂ and
327 climate) to the final year of each climate forcing dataset. Note that the NCC climate forcing
328 data is only available until 2000 while the Princeton GPCC data runs until 2010.

329 2.5 Model evaluation and analysis of simulation results

330 We started by evaluating the hydrology, concentrating on flooded area as this was
331 underestimated in the original ORCHILEAK model set up (Lauerwald et al., 2017). The new
332 MFF and MFS forcing files meant that we had to re-evaluate both discharge and floodplain
333 inundation dynamics. We firstly focused on recreating observed discharge at Obidos (Fig.
334 S1), the most downstream gauging station for which an observed time-series is available
335 (Cochonneau et al., 2006). Total flooded area of the central quadrant of the Amazon basin
336 (Fig. S1) was tested against remote sensing data (Melack et al., 2011). Note that the Melack
337 et al. dataset uses the same wetland mask as we use here, but the seasonality and area of
338 inundation is completely independent. We then performed a model validation for the DOC
339 and aquatic CO₂ evasion fluxes using the same validation data and methodology as described
340 in Lauerwald et al. (2017), as well as an in-depth comparison of our results to those of
341 previous studies. In addition, we examined the interannual variation of both the terrestrial
342 (meaning NPP and SHR) and aquatic C fluxes (also referred to as LOAC fluxes, and meaning
343 CO₂ evasion from the water surface and the export flux of C to the coast) of the Amazon, and
344 assessed how this variation relates to rainfall and temperature variation through linear
345 regression analysis. As we found long-term (decadal) trends in several of the fluxes, most
346 notably NPP (Tables S2 & S3), we detrended the annual times series using the Detrend
347 function within the “SpecsVerification” package in R (R Core Team 2013), before
348 performing the regression analyses using STATISTICA™. Finally, we sum the various C

349 fluxes to calculate the net C balance of the Amazon Basin (see 2.6) and examine the
350 importance of the LOAC fluxes to the overall C balance.

351 2.6 Calculating the net carbon balance of the Amazon

352 In order to estimate the net C balance of the Amazon basin, we summed the terrestrial and
353 aquatic C fluxes to estimate Net Ecosystem Production (NEP) and Net Biome Production
354 (NBP). Positive values of NEP and NBP correspond to a net sink.

355 We define NEP as follows:

$$356 \quad \quad \quad NEP = NPP + TF - SHR - FCO_2 - LE_{Aquatic} \quad (1)$$

357 Where *NPP* is terrestrial net primary production, *TF* is the throughfall flux of DOC, *SHR* is
358 soil heterotrophic respiration (only the part evading from the soil surface); *FCO₂* is CO₂
359 evasion from the water surface and *LE_{Aquatic}* is the export flux of C to the coast. *NBP* is the
360 same as *NEP* but with the addition of the C lost (or gained) through land use change (*LUC*,
361 including fires and the export of woody biomass) and crop harvest (*Harvest*):

$$362 \quad \quad \quad NBP = NEP - (LUC + Harvest) \quad (2)$$

363

364 3. Results

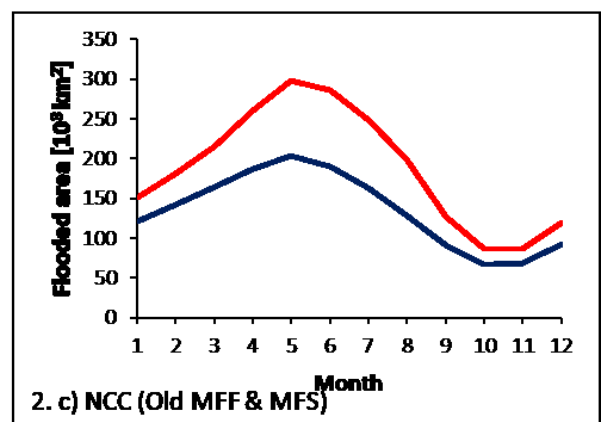
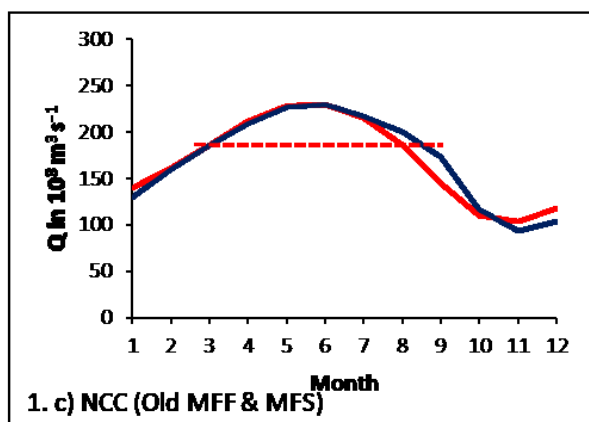
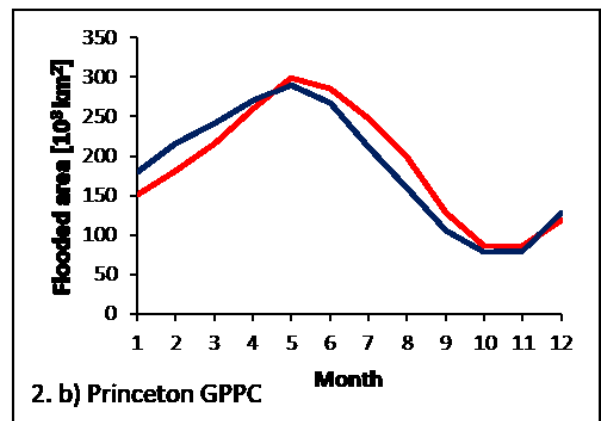
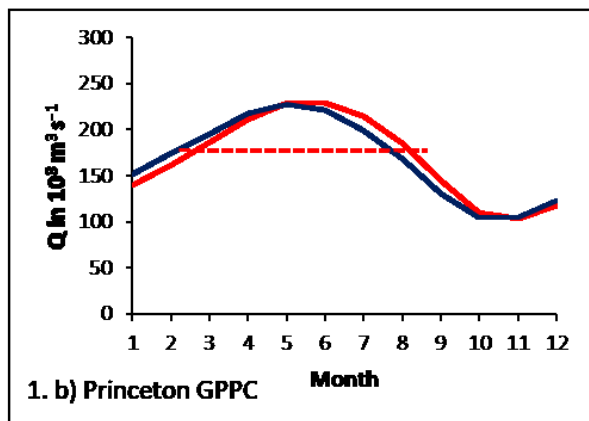
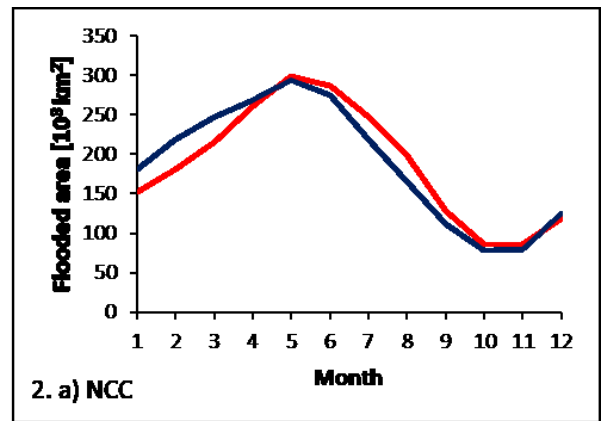
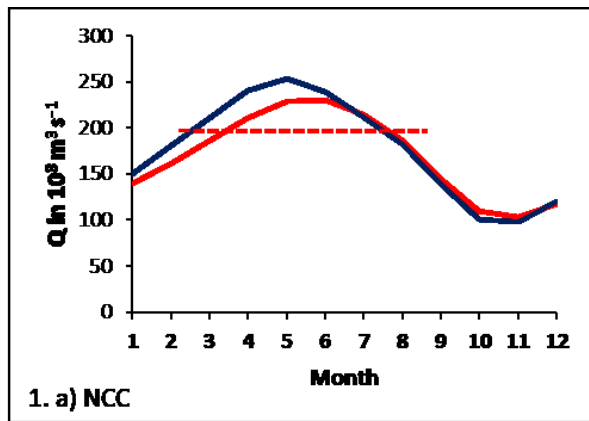
365 3.1 Representation of Hydrology

366 The model is able to reproduce river discharge at Obidos (1980-2000), the farthest
367 downstream river gauge (Fig. S1), both in terms of total magnitude and seasonal variability.
368 Simulation with the old floodplain/swamp forcing used by Lauerwald et al. (2017) and
369 simulations based on the new floodplain/swamp forcing file showed a similarly good
370 performance (Fig.3-1 a-c, Table 1). There was no substantial difference in the simulated

371 discharge from the Amazon basin after the implementation of the new floodplain. However,
372 the new floodplain forcing substantially improved the ability of the model to reproduce the
373 seasonality in flooded area (Fig. 3-2a-c); Nash Sutcliffe-Efficiency (NSE) and Root Mean
374 Square Error (RMSE) were 0.91 and 12% respectively with the new floodplain forcing,
375 compared to -0.75 and 32% with the old (Table 1).

376 Comparing model runs driven by the two different climate forcing, NCC and Princeton
377 GPCP climate data, we find a similarly good performance as well. With both forcing data
378 sets, we were able to recreate the observed mean magnitude and seasonality in discharge at
379 Obidos (1980-2000) (Fig. 3-1 a, b) and flooded area in the central (Fig. S1) Amazon (1981-
380 1996) (Fig. 3-2 a, b).

381 While the model was mostly able to reproduce the observed interannual variation in
382 discharge, there was some minor difference in performance related to the choice of climate
383 forcing (Figure 4, Table S1). The simulation driven by the Princeton GPCP data had an NSE
384 of 0.79 and a RMSE of 4% against observations, compared to 0.50 and 7% for the NCC run
385 (Figure 4, Table S1). The year with the highest observed discharge was 1989 with a mean of
386 $199 \cdot 10^3 \text{ m}^3\text{s}^{-1}$. The Princeton GPCP run correctly simulated 1989 as the year with the highest
387 discharge, with a mean of $194 \cdot 10^3 \text{ m}^3\text{s}^{-1}$. The NCC run ranks 1989 as the year with the
388 second highest discharge, and actually predicts a higher 1989 mean discharge of $203 \cdot 10^3 \text{ m}^3\text{s}^{-1}$
389 ¹. With NCC, the year with highest discharge is 1982, which is the 5th highest discharge in
390 the observed time series. Conversely, the NCC simulation correctly modelled 1992 as the
391 year with the lowest discharge ($146 \cdot 10^3 \text{ m}^3\text{s}^{-1}$) while the run driven with Princeton ranked
392 1992 second lowest (Figure 4, Table S1). It is important to note that the differences in
393 observed discharge between both the highest (1989) and second highest (1994), and lowest
394 (1992) and second lowest (1983) are minor (Figure 4, Table S1).



395

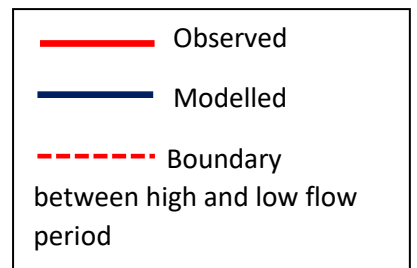
396

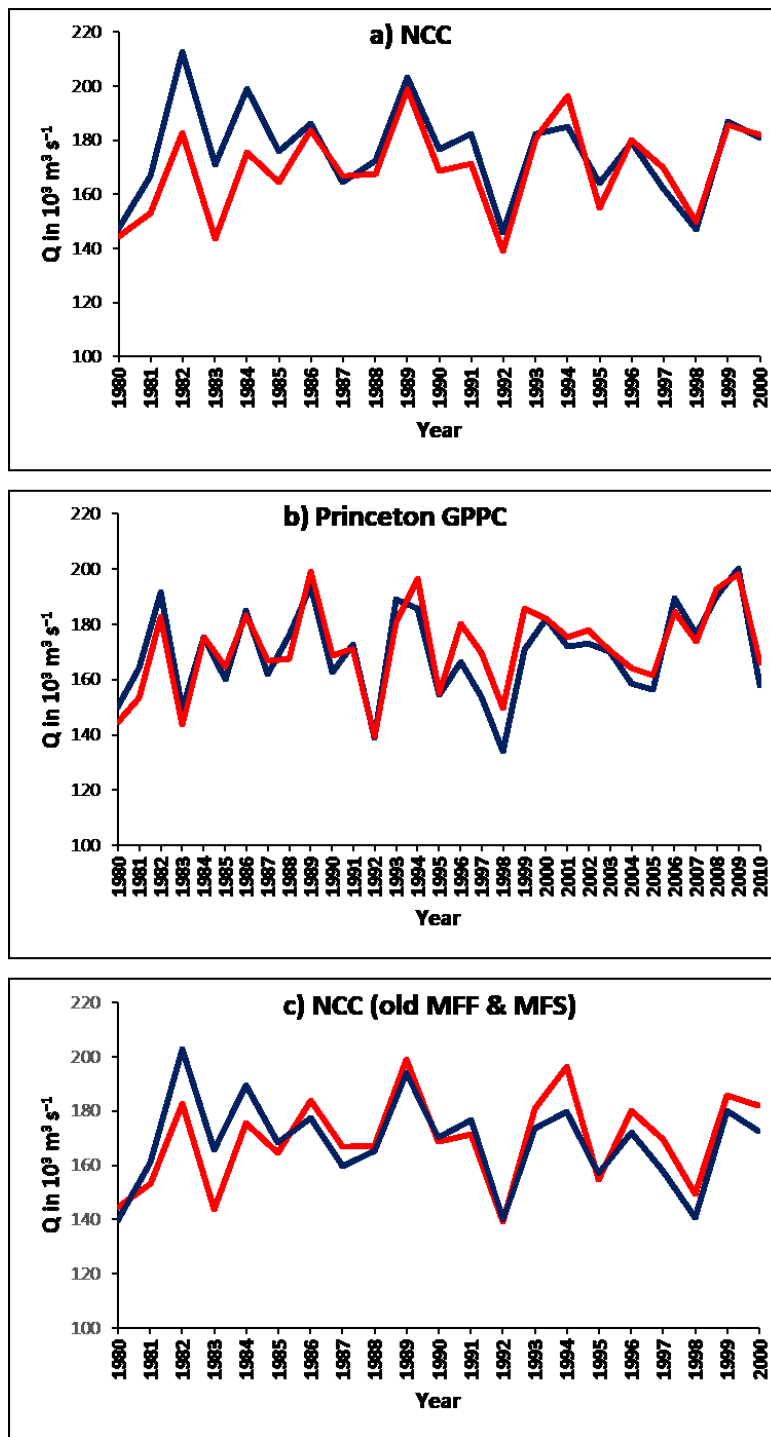
397

398

399

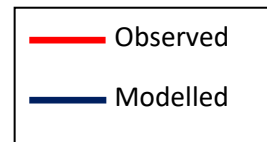
Figure 3- 1: Seasonality of simulated *versus* observed discharge (Cochonneau et al., 2006) at Obidos (1980-2000 monthly mean), with a) NCC climate forcing with standard MFF b) Princeton GPPC climate forcing with standard MFF and c) NCC with old MFF & MFS. 2: Seasonality of simulated versus observed flooded area (Melack et al., 2011) in the central Amazon basin (1981-1996 monthly mean) with a) NCC climate forcing with standard MFF b) Princeton GPPC climate forcing with standard MFF and c) NCC with old MFF & MFS.





400
 401
 402
 403
 404
 405
 406

Figure 4. Annual variation of simulated vs observed discharge (Cochoneau et al., 2006) at Obidos (1980-2000) for a); run with NCC climate forcing with standard MFF, b) Princeton GPPC climate forcing with standard MFF and c) NCC climate forcing with old MFF & MFS



407
 408
 409
 410
 411
 412

Table 1. Performance statistics for modelled versus observed discharge Q at Obidos and flooded area in the central Amazon basin for different climate forcing configurations

Climate forcing	Seasonality in Q at Obidos (1980-2000)			Flooded area in central Amazon (1981-1996)			Interannual variation in Q at Obidos (1980-2000)		
	RSME	NSE	R ²	RSME	NSE	R ²	RSME	NSE	R ²
NCC	9%	0.91	0.95	12%	0.91	0.91	7%	0.50	0.66
Princeton GPCC	6%	0.94	0.95	13%	0.89	0.90	4%	0.79	0.81
NCC (old MFF & MFS)	6%	0.95	0.95	32%	-0.75	0.97	6%	0.62	0.67

413

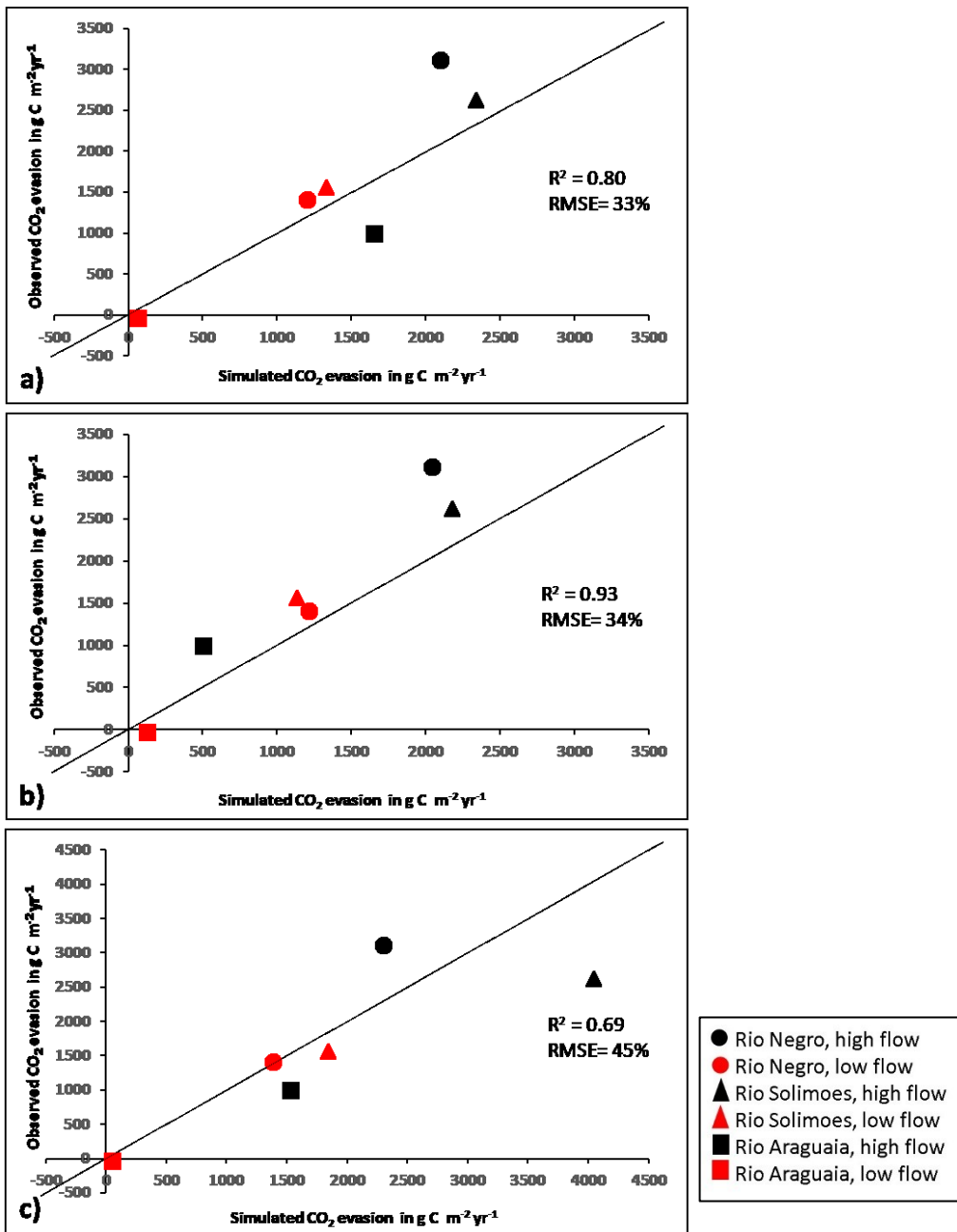
414 3.2 Carbon fluxes along the Amazon Basin

415 We estimate a long-term mean (1980-2000 across six model runs) NPP rate of 1,214 (1,204-
 416 1,223) g C m⁻² yr⁻¹ (range represents the variation caused by the combination of the two
 417 climate forcing and the three MFF forcing files; standard, MFF +7 and MFF-7), amounting to
 418 a total NPP of 6.81 (6.75-6.86) Pg C yr⁻¹ for the entire Amazon Basin (5.6 x 10⁶ km²). If we
 419 only consider the uncertainty associated with climate forcing alone, the range is reduced to
 420 6.77-6.85 Pg C yr⁻¹. The effect of the new MFF and MFS on NPP was negligible; mean
 421 annual NPP being 1,220 g C m⁻² yr⁻¹ (total of 6.84 Pg C yr⁻¹) and 1,222 g C m⁻² yr⁻¹ (total of
 422 6.85 Pg C yr⁻¹) with the original (Lauerwald et al., 2017) and new forcing files, respectively,
 423 both driven by NCC. We estimate a mean annual soil heterotrophic respiration (SHR) of 5.87
 424 (5.62-6.16) Pg C yr⁻¹. The new forcing file had a significantly greater effect on SHR than on
 425 NPP; the original forcing file (with NCC) produces a higher mean annual SHR of 6.30 Pg C

426 yr⁻¹, compared to 5.94 Pg C yr⁻¹ (with NCC) this difference due to the greater suppression of
427 organic matter decomposition with the new MFF (Rueda-Delgado et al., 2006). We estimate
428 a mean annual throughfall DOC flux (TF) of 79 (78-79) Tg C yr⁻¹.

429 We simulate a mean annual (1980-2000) CO₂ evasion of 746 (526-998) Tg C yr⁻¹ from the
430 water surfaces of the Amazon basin, a 97% increase from the 379 Tg C yr⁻¹ produced with
431 the original ORCHILEAK configuration (Lauerwald et al., 2017). If we only include the
432 uncertainty associated with climate forcing, we produce a mean of 729 Tg C yr⁻¹ and the
433 range is substantially reduced to 700-758 Tg C yr⁻¹, meaning that the majority of the
434 uncertainty in the evasion flux comes from the MFF forcing. We attribute approximately 75%
435 of the CO₂ evasion flux to the floodplain compared to 51% in the original study (Lauerwald
436 et al., 2017). With the new MFF forcing, we moderately improved the reproduction of
437 observed CO₂ evasion fluxes during low (monthly avg. discharge < yearly avg. discharge)
438 and high flow (monthly avg. discharge > yearly avg. discharge) periods at three sites in the
439 Amazon (Rasera et al., 2013, Fig. 5) ($R^2=0.80$, $RMSE = 1.4 \mu\text{mol CO}_2 \text{ m}^{-2} \text{ s}^{-1}$ vs $R^2=0.69$,
440 $RMSE = 1.9 \mu\text{mol CO}_2 \text{ m}^{-2} \text{ s}^{-1}$, with new (a) and old MFF (c) respectively, both driven by
441 NCC). The performance was further improved with the Princeton GPCC climate data; R^2
442 $=0.93$, $RMSE = 1.4 \mu\text{mol CO}_2 \text{ m}^{-2} \text{ s}^{-1}$ (Fig. 5, b).

443



444

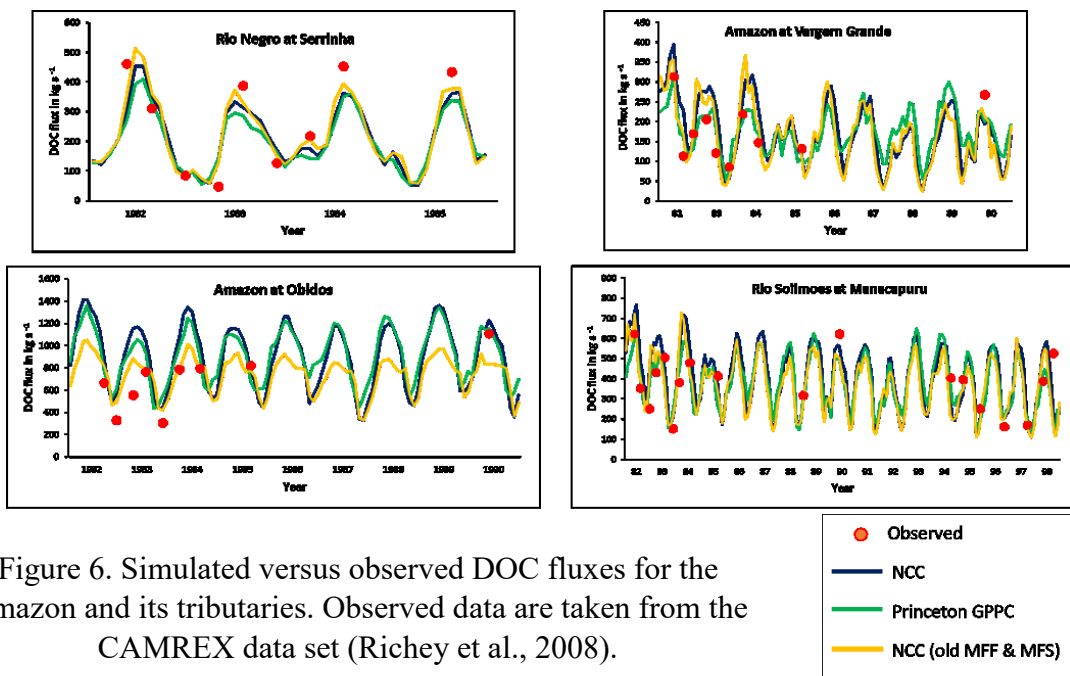
445 Figure 5. Observed versus simulated CO₂ evasion rates per water surface area for a); run
 446 with NCC climate forcing (standard MFF), b) Princeton GPCC climate forcing (standard
 447 MFF) and c) NCC climate forcing with old MFF & MFS. Observed data are from Rasera
 448 et al. (2013). Reported are means of the observed values, 2006 -2010. The simulated
 449 values refer to the mean evasion rate during low (monthly avg. discharge < yearly avg.
 discharge) and high flow periods (monthly avg. discharge > yearly avg. discharge) (1981–
 2000), see Figure 3. Note that the scale of the axes c) is slightly different to a) and b).

450 We simulate a mean annual (1980-2000) DOC export to the coast (downstream of Obidos) of

451 38 (33-44) Tg C yr⁻¹. In Figure 6, we compare simulated DOC flux against the observations

452 at several sites (see Fig. S1 for locations) and find that the model can recreate the temporal

453 variation in DOC relatively well (Table S5). The effect of the new forcing files is mixed, with
 454 the performance improving at some sites but worsening at others (Fig. 6). The largest impact
 455 can be seen at Obidos where the new forcing files result in a substantially larger DOC flux
 456 during high flow. The model run using the old MFF and MFS appears to perform better at
 457 moderate discharge, while the new set up appears to perform better during periods when
 458 observed DOC is very high (i.e. 1990). Both appear to overestimate DOC flux at Obidos
 459 during low flow. We simulate a mean annual flux (to the coast) of dissolved CO₂ of 7.1 (6.8-
 460 7.7) Tg C yr⁻¹.



461
 Figure 6. Simulated versus observed DOC fluxes for the Amazon and its tributaries. Observed data are taken from the CAMREX data set (Richey et al., 2008).

462
 463
 464

465 3.3 The net carbon balance of the Amazon Basin

466 The long-term mean (1980-2000) C balance; that is the components of the Net Ecosystem
 467 Production (NEP, equation 1), is presented in Fig. 7. We estimate a mean (1980-2000) NEP
 468 of 0.23 (0.15-0.33) Pg C yr⁻¹ and a mean Net Biome Production (NBP, equation 2) of 0.04 (-

469 0.04-0.14) Pg C yr⁻¹. Using the original floodplain and swamp forcing files (with NCC), we
 470 estimate a mean annual NEP of 0.17 Pg C yr⁻¹. Using the same set up (with NCC) but with
 471 the new MFF and MFS forcing files we produce a higher sink of 0.21 Pg C yr⁻¹.

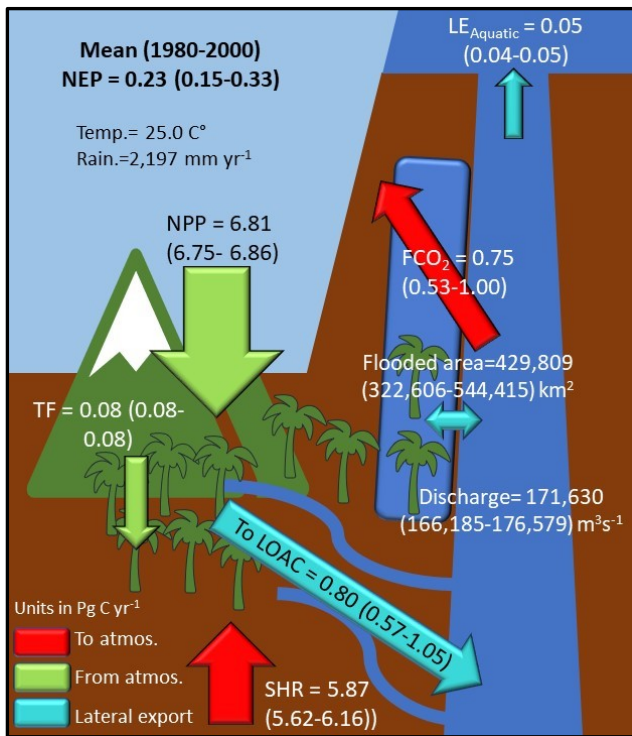


Figure 7. Simulated annual C budget (NEP) for the Amazon basin annual mean (1980-2000), where NEP is net ecosystem production, NPP is terrestrial net primary productivity, TF is throughfall, SHR is soil heterotrophic respiration, FCO_2 is aquatic CO_2 evasion, LOAC is C leakage to the land-ocean aquatic continuum (FCO_2 + to coast), and $LE_{Aquatic}$ is the export C flux to the coast. Numbers refer to mean across the six simulations while numbers in parentheses refer to range.

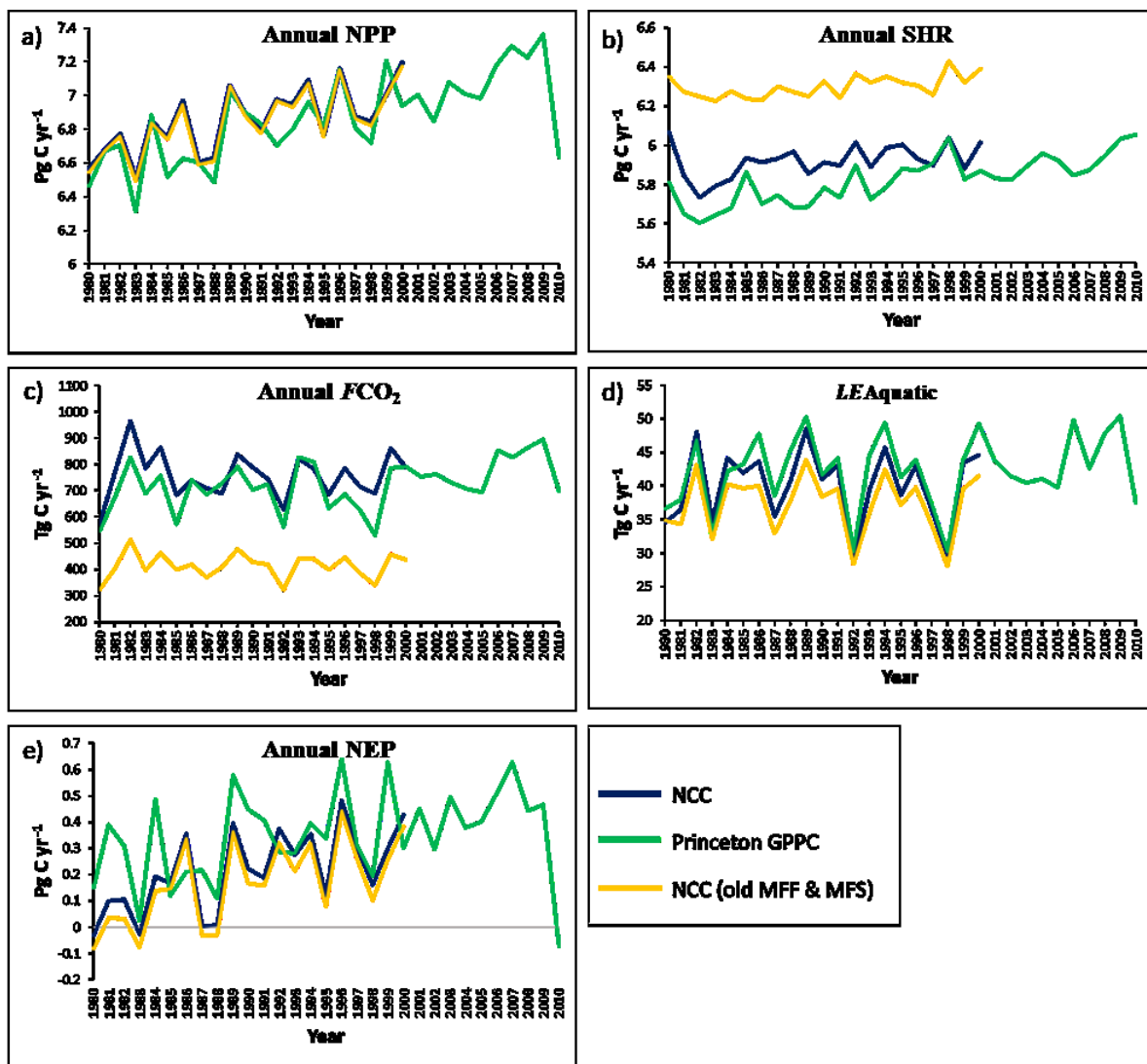
472

473 3.4 Interannual variation of the C fluxes within the Amazon Basin

474 Our results show considerable interannual variation in NPP, from a mean low of 6.41 (6.29-
 475 6.52) Pg C yr⁻¹ in 1983, to a high of 7.16 (7.14- 7.16) Pg C yr⁻¹ in 1996 (Fig.8-a), though the
 476 Princeton GPCC simulation, which runs until 2010, has several years (2006-2009 inclusive)
 477 with slightly higher NPP. This variation has a strong positive correlation with precipitation
 478 (detrended $R^2 = 0.48$, $p < 0.001$ with NCC; detrended $R^2 = 0.43$, $p < 0.0001$ with Princeton
 479 GPCC, Table S6 & S7, Fig. 9-a) and a strong negative correlation with temperature
 480 (detrended $R^2 = 0.56$, $p < 0.0001$ with NCC; detrended $R^2 = 0.43$, $p < 0.0001$ with Princeton
 481 GPCC, Table S6 & S7, Fig. 9-b). In addition, NPP is inversely correlated with the
 482 multivariate ENSO index (MEI, sum of monthly MEI from July of preceding year to June of
 483 concurrent year, detrended $R^2 = 0.40$, $p < 0.01$ with NCC; detrended $R^2 = 0.35$, $p < 0.001$ with

484 Princeton GPPC, Table S6 & S7, Fig. 9-c) (Wolter et al., 2011). We also find substantial
 485 interannual variation in SHR from a mean (across the two runs with new floodplain forcing)
 486 low of 5.69 (5.41- 6.03) Pg C yr⁻¹ in 1982 to a high of 6.06 (5.91- 6.24) Pg C yr⁻¹ in 1998
 487 (Fig. 8-b). Conversely to NPP, SHR is positively correlated with temperature, and negatively
 488 correlated with rainfall, though these relationships are relatively weak (relationship with
 489 temperature not significant with NCC, detrended temperature R²= 0.13 with Princeton
 490 GPPC, p<0.05; detrended rainfall R²=0.19, p<0.05 with NCC, detrended rainfall R² = 0.24,
 491 p<0.01 with Princeton GPPC).

492



499 Figure 8. Simulated annual variation in NEP and its components over the Amazon Basin
500 from 1980-2000 (2010 in case of Princeton GPCC).

501

502 Our results also show considerable inter-annual (1980-2000) variation in inland water CO₂
503 evasion from a mean low of 571 (402- 759) Tg C yr⁻¹ in 1980 to a high of 920 (633- 1,267)
504 Tg C yr⁻¹ in 1982 (Fig.8-c), strongly correlated with precipitation (detrended R² = 0.55,
505 p<0.001 with NCC; detrended R² = 0.64, p<0.0001 with Princeton GPCC, Table S6 & S7)
506 and inversely correlated with temperature (detrended R² = 0.21, p<0.05 with NCC; detrended
507 R² = 0.18, p<0.05 with Princeton GPCC, Table S6 & S7). While both model runs rank 1982
508 as having the highest CO₂ evasion over the simulation period (1980-2000), there is some
509 divergence in regards to the lowest ranking year. The NCC run ranks 1980 lowest with 584
510 (422-759) Tg C yr⁻¹ whereas the Princeton GPCC run ranks 1998 lowest with a total of 538
511 (399-685) Tg C yr⁻¹. In 1980 the Amazon rainy season was exceptionally dry (Andreoli et
512 al., 2012), while 1998 coincides with a strong El Nino event (Fig.9-c) and associated
513 anomalously low precipitation and high temperatures (Wenhong et al., 2011; Gloor et al.,
514 2013, 2015). Conversely, 1982 experienced an exceptionally wet rainy season (Andreoli et
515 al., 2012). These temporal patterns are also exhibited in the rainfall and temperature
516 parameters from both of the climate forcings used in this study (Fig.9).

517 At the interannual timescale, aquatic CO₂ evasion is only weakly to moderately correlated
518 with NPP (detrended R² = 0.19, p<0.05 NCC run; detrended R² = 0.28, p<0.01 with
519 Princeton GPCC run, Table S6 & S7) and therefore the proportion of NPP lost through the
520 LOAC is variable, ranging from 9% to 13%. In contrast, inland water CO₂ evasion is strongly
521 inversely correlated with SHR (detrended R² = 0.76, p<0.0001 NCC run; detrended R² =
522 0.66, p<0.0001 with Princeton GPCC run, Table S6 & S7), indicating that years with less
523 SHR have more evasion, and vice versa. Again, we find considerable interannual variation in

524 C flux to the coast (Fig. 8 d) displaying a similar pattern to aquatic CO₂ evasion (aquatic CO₂
525 evasion *versus* C flux to coast R² =0.48 for NCC, p<0.001; R² =0.64 p<0.0001 for Princeton
526 GPC, Table S6 & S7). Overall, and in relative terms, the LOAC fluxes show far greater
527 interannual variation than the terrestrial C fluxes. For example, aquatic CO₂ evasion (NCC,
528 1980-2000) has a coefficient of variation (CV) of 11.7%, while the lateral flux of C to the
529 coast has a CV of 13.6%. In contrast, NPP and SHR have a CV of only 2.9% and 1.5%,
530 respectively.

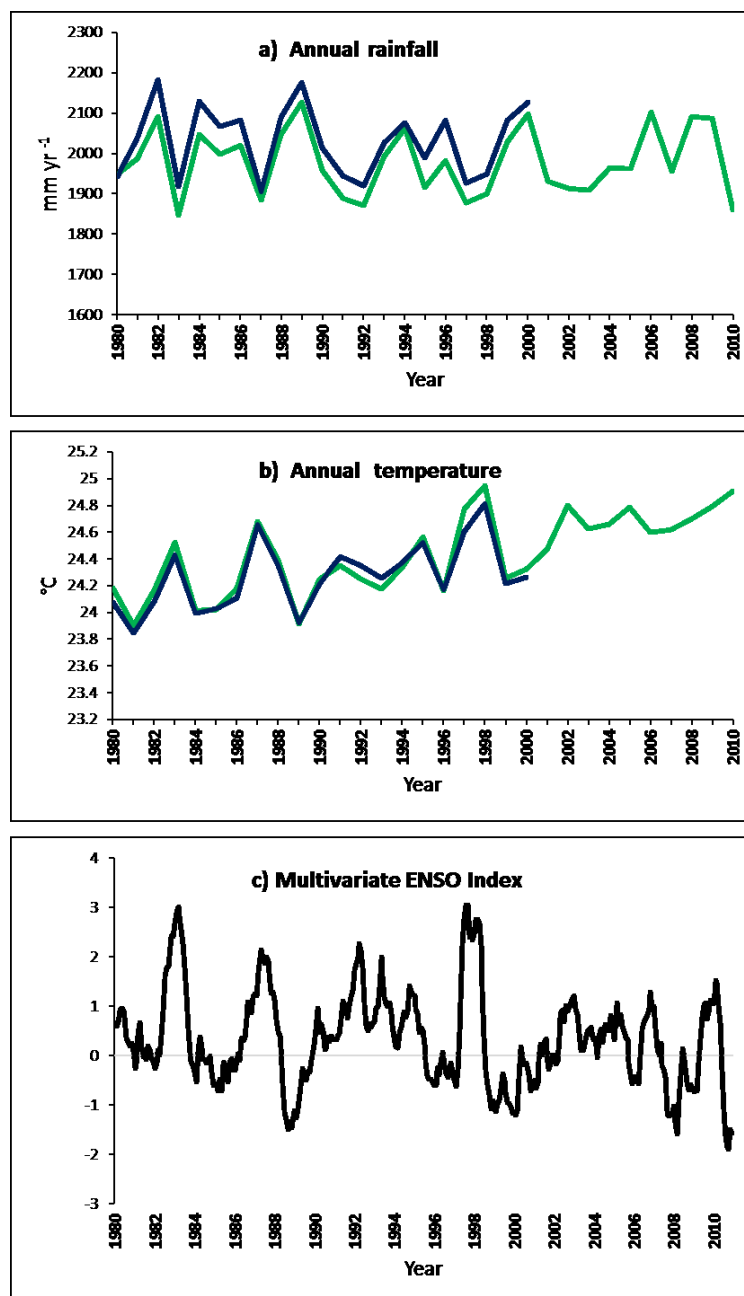


Figure 9. Interannual variation in a) rainfall and
b) temperature. c) Monthly multivariate ENSO
Index from 1980-2010 (Wolter et al., 2011)



532
533
534
535 As with its constituent components, simulated NEP shows considerable interannual variation
536 (Figure 8-e) from a low of -0.05 (-0.11 – 0.03) Pg C yr⁻¹ in 1983 to a high of 0.52 (0.41- 0.64)
537 Pg C yr⁻¹ in 1996. NEP is positively correlated with rainfall (detrended R² = 0.27, p<0.05
538 NCC run; detrended R² = 0.25, p<0.01 with Princeton GPCC run, Table S6 & S7) and
539 negatively correlated with temperature (detrended R² = 0.45, p<0.001 NCC run; detrended R²
540 = 0.41, p<0.001 with Princeton GPCC run, Table S6 & S7). The association with ENSO
541 (detrended R² = 0.35, p<0.01 NCC run; detrended R² = 0.26, p<0.01 with Princeton GPCC
542 run, Table S6 & S7) can be clearly seen in the simulated time series of NEP. Of the top six
543 years with the lowest NEP (largest source of C to the atmosphere), four coincide with strong
544 El Nino events, namely 1983, 1988, 1987 and 1998. Conversely, several of the years with the
545 highest NEP (largest sink of atmospheric CO₂) take place during La Nina events, notably the
546 strong La Nina event of 1988-1989, which results in the second highest simulated NEP; note
547 that 2011 was one of the strongest La Nina on record but is not included in our forcing
548 period. Taking the Princeton GPCC run alone, 2010 has the lowest NEP being a net CO₂
549 source to the atmosphere of -0.12 Pg C yr⁻¹ (-0.14- -0.07) and coincides with another El Nino
550 event combined with anomalously high Atlantic sea surface temperatures (SSTs) (Lewis et
551 al., 2011).

552 We diagnosed the covariance between aquatic CO₂ evasion and the terrestrial C balance
553 (defined as NPP-SHR) to determine how the variance in aquatic CO₂ evasion contributes to
554 the overall variance in NEP across the simulation period. We find a negative covariance
555 between aquatic CO₂ evasion and the terrestrial C balance of -0.024 and -0.022 for NCC and
556 Princeton GPCC, respectively. Moreover, the terrestrial C balance is substantially more

557 sensitive to changes in both precipitation and temperature than NEP (Tables S8-S11). For
558 example (NCC run, Table S8), across the Amazon basin we find that the terrestrial C balance
559 increases by 120 Tg C yr⁻¹ for every 100mm increase in rainfall, while NEP only increases by
560 57 Tg C yr⁻¹. Note that these values are based on simple linear regression and thus the
561 sensitivity to rainfall may be exaggerated but this is the case for both values.

562 As a consequence of this change in sensitivity, the variation of the budget is less pronounced
563 once the aquatic components are incorporated; the terrestrial C balance has a SD of 0.20 Pg C
564 yr⁻¹ and 0.24 Pg C yr⁻¹ with NCC and Princeton GPCC respectively, while NEP has a SD of
565 0.15 Pg C yr⁻¹ and 0.17 Pg C yr⁻¹. These results concur with the idea of CO₂ evasion having a
566 moderating effect on overall heterotrophic respiration and suggest that accounting for CO₂
567 evasion from the river-floodplain network dampens the interannual variation in NEP.

568

569 4. Discussion

570 Our value of mean (across two models) NPP rate of 1,214 g C m⁻² yr⁻¹ matches closely to
571 previous estimates in the Amazon. Rodig et al. (2018) estimated a mean annual NPP of 1,130
572 g C m⁻² yr⁻¹ using the forest gap FORMIND model, while a value of 1,030 g C m⁻² yr⁻¹ was
573 derived from MODIS remote-sensing data (Zhao & Running, 2010).

574 Our estimate of mean total annual aquatic CO₂ evasion of 746 (526-998) Tg C yr⁻¹ is
575 relatively close to the 800 Tg C yr⁻¹ proposed by Rasera et al. (2013) from upscaling of
576 observations, over a larger basin area of 6 × 10⁶ km². If we adjust our estimate (calculated
577 across a smaller basin area of 5.6 × 10⁶ km²) to the same area, then we get a closer estimate
578 of 799 Tg C yr⁻¹. Moreover, if we only base our mean CO₂ evasion estimate on the same
579 years as Rasera et al. (i.e. 2006- 2010), we actually produce a larger value of 887 Tg C yr⁻¹
580 (based on Princeton GPCC run only). We also estimate a similar distribution of CO₂ evasion

581 between low and high flow periods (Table S4). Like those of Rasera et al. (2013), our results
582 exhibit a strong seasonal cycle in CO₂ evasion, with the high flow season (monthly avg.
583 discharge > yearly avg. discharge) contributing approximately 75% of the annual total. In
584 contrast, our results are considerably higher than those of Richey et al. (Table S4). It is
585 encouraging that our results are similar to those of Rasera et al. (2013) as their upscaling was
586 based on an extensive 5-year field campaign where the flux of CO₂ was directly measured
587 while those of Richey et al. (2002) were derived indirectly from *p*CO₂ measurements. In
588 terms of flood extent, the Rasera et al. study used the same assumptions for water surface
589 area as Richey et al (2002), who in turn used an older version (Hess et al., 2002) of the Hess
590 et al. (2015) floodplain product use in this study.

591 For the central quadrant of the Amazon basin alone (area = 1.77×10^6 km²), we simulate a
592 mean annual aquatic CO₂ evasion (1980-2000) of 341 and 318 Tg C yr⁻¹ with NCC and
593 Princeton GPPC, respectively, close to the 360 Tg C yr⁻¹ estimated by Rasera et al. (2013),
594 but considerably higher than the 210 Tg C yr⁻¹ of Richey et al. (2002) and the 229 Tg C yr⁻¹ of
595 Lauerwald et al. (2017). Our results concur with both previous upscaling studies that the
596 central Amazon basin contributes approximately 45% of the basin wide aquatic CO₂ evasion
597 (Table S4). The differences between our CO₂ evasion estimates and those of Richey et al.
598 (2002) are largely due to gas exchange velocity; we applied a fixed k_{600} rate of 3.5 m day⁻¹ for
599 rivers, while they used very conservative gas exchange velocities of 1.2 to 2.3 m day⁻¹.
600 Conversely, the differences between our results and those of Lauerwald et al. (2017) are
601 largely a result of the increase in maximal fraction of floodplain (MFF) across the basin, and
602 the resultant increase in direct C inputs to inundated areas from canopy through-fall,
603 submerged litter and soils. Our estimated DOC export to the coast (downstream of Obidos) of
604 34 (34-44) Tg C yr⁻¹ is relatively high; Lauerwald et al. (2017), Richey et al. (1990) and

605 Moreira-Turcq et al. (2003) estimated this flux at 23.4 Tg C yr⁻¹ , 24.4 Tg C yr⁻¹ and 27 Tg C
606 yr⁻¹, respectively.

607 Our results for the mean NEP of 0.23 (0.15-0.33) generally concur with previous estimates.
608 Tian et al. (1998) used the Terrestrial Ecosystem Model to estimate a mean annual NEP,
609 without considering the LOAC loop of the carbon cycle (undisturbed ecosystems, 1980-
610 1994), of 0.2 ±0.9 Pg C yr⁻¹. Another modelling study (S. Sitch, B. Smith and J. Kaplan,
611 unpublished but cited in Prentice and Lloyd, 1998, page 620) also settled on a mean annual
612 NEP of around 0.2 ±1.2 Pg C yr⁻¹ over the same 15-year period. A 2016 review (Grace,
613 2016), compiled all of the existing literature to produce two estimates of the net C balance of
614 the Amazon Basin; one ‘bottom-up’ approach using “plot data and remote sensing” and one
615 ‘top-down approach’ using “aircraft-based measurements in the planetary boundary layer”,
616 the latter based on Gatti et al. (2014). These two approaches include perturbation fluxes such
617 as deforestation and harvesting and evasion emissions in the atmospheric inversion estimate
618 of Gatti et al. and are thus equivalent to our estimate of NBP. The bottom-up approach
619 concludes that the Amazon Basin is a net C source to the atmosphere of 0.11 Pg C yr⁻¹ when
620 including land use change emissions but with an uncertainty of ± 0.16, in other words not
621 markedly different from zero. The top-down approach came to a similar conclusion; that the
622 Amazon is a net source to the atmosphere of only 0.06 Pg C yr⁻¹ in a ‘normal year’ but only
623 two years (2010 and 2011) were analyzed in Gatti et al. Again, the near neutral balance of
624 Gatti et al. (2014) intrinsically includes aquatic CO₂ evasion (though not the lateral fluxes of
625 C to the coast). They argue that the impact of riverine CO₂ evasion on the Amazon C balance
626 is minimal as the “riverine organic carbon loop is very nearly closed”. In other words, the
627 vast majority of LOAC export to aquatic systems return to the atmosphere before leaving the
628 Amazon Basin. In summary, the results of Gatti et al. (2014) are arguably the most
629 comparable to our own and it is therefore encouraging that we produce a relatively similar

630 NBP of 0.04 (-0.04-0.14) Pg C yr⁻¹ (a difference of 100 Tg C⁻¹ but with overlapping
631 uncertainty ranges). It is important to note that ORCHILEAK does not incorporate methane
632 fluxes. Indeed, if we include the recent estimate of the annual methane flux of approximately
633 40 Tg C⁻¹ (Pangala et al., 2017) measured from the lower troposphere via aircraft; our NBP
634 reduces to a neutral C balance.

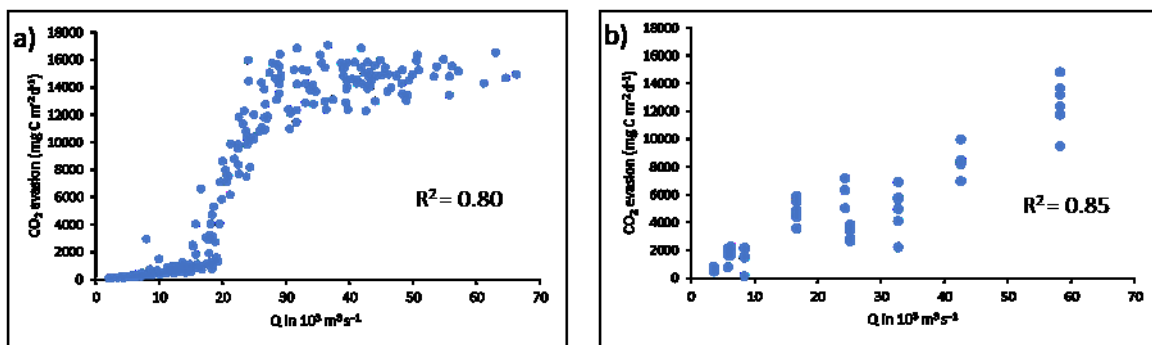
635 While the new maximal fraction of floodplain (MFF) forcing leads to a dramatic increase in
636 aquatic CO₂ evasion, it actually causes an overall decrease in the flux of CO₂ from the entire
637 Amazon basin to the atmosphere. The greater inundation leads to a reduction in
638 decomposition rates of litter, and soil organic matter. This suppression of organic matter
639 decomposition has been observed in further field experiments (Dos Santos & Nelson, 2013),
640 in addition to the study that informed the model configuration (Rueda-Delgado et al., 2006).
641 This means that there is an additional net land C sink of approximately 40 Tg C yr⁻¹ per year
642 with the new floodplain compared to the old floodplain. While in a single year these
643 differences are not so substantial, over long time periods they could lead to significant
644 differences in the long-term net C balance of the Amazon.

645 We found that the interannual variation in NPP is positively correlated with rainfall and
646 negatively correlated with temperature and our results concur with previous research showing
647 that drought years have significantly lower NPP. In our outputs, two of the years with the
648 lowest NPP are 1983 and 1988, coinciding with two strong El Nino events (1982-1983 and
649 1987-1988, Figure 9), and corroborating the findings of Asner & Townsend (2000) based on
650 analysis of remote sensing data from 1982-1993. Previous modelling studies such as Botta et
651 al (2002) have also found 1983 and 1988 to be years with anomalously low NPP in the
652 Amazon. Moreover, a 2011 study that combined remote sensing and modelling (Potter et al.,
653 2011) estimated that the 2010 drought caused a reduction in NPP in the Amazon of 7%
654 relative to the La Nina year 2008, and we produce a similar value of 8% (0.58 Pg C).

655 However, a more recent study (Doughty et al., 2015) contradicts these findings. Doughty et
656 al. (2015) measured NPP, autotrophic respiration and heterotrophic respiration at thirteen 1ha
657 plots across South America from 2009-2011 and found that NPP remained relatively constant
658 throughout the period. They observed a reduction in CO₂ uptake via photosynthesis by 0.38
659 Pg C yr⁻¹ during the 2010 drought, but this was offset by a concurrent reduction in
660 autotrophic respiration. They observed that the trees prioritised investment in growth (canopy
661 tissue), while they reduced autotrophic respiration investment in tissue maintenance and
662 defence, which ultimately may have caused an increase in tree mortality post drought
663 (Doughty et al., 2015). The inability of dynamic global vegetation models (DGVMs), as well
664 as remote sensing driven algorithms (Zhao & Running, 2010; Medlyn, 2011; Wang et al.,
665 2013) to represent these complex biological interactions is a major limitation in current
666 efforts to estimate NPP at the regional to global scale.

667 Our results show that both the seasonality and interannual variation in aquatic CO₂ evasion,
668 are closely correlated with discharge. In Figure 10 a) we show the relationship between
669 simulated monthly discharge and CO₂ evasion on the Madeira River at Porto Velho (R²=0.81)
670 (see Fig. S1 for location). The Madeira basin contains approximately one fourth of
671 Amazonian wetlands (Melack and Hess 2010), including the extensive Llanos de Moxos and
672 was the subject of a recent CO₂ evasion field campaign (Almeida et al., 2017). Our
673 relationship follows a sigmoid curve where aquatic CO₂ evasion increases slowly at first
674 while discharge remains in bank. Once the river over-tops its banks, CO₂ evasion increases
675 rapidly before levelling out once the full area of the floodplain is saturated. Thus, at the basin
676 scale, aquatic CO₂ evasion not only increases because of larger floodplain surface area, but
677 also because of higher areal rates. This highlights the disproportionate importance of
678 floodplains as a source of C and supports the findings of Almeida et al. (2017, Fig. 10, b).
679 While they found a similarly strong relationship between observed discharge and aquatic CO₂

680 evasion at Porto Velho ($R^2=0.85$), as well as a similar range of values, the relationship does
 681 not follow precisely the same shape as ours. Their increase in evasion rate is more gradual
 682 and they do not observe a plateauing of CO₂ evasion above a certain discharge. This perhaps
 683 suggests that we underestimate the maximum extent of the floodplain in this specific model
 684 grid, and indeed, the location of Porto Velho, is in the minority of model grids where the
 685 maximum inundation actually decreases with the implementation of the new MFF forcing
 686 file.



687
 688
 689 Figure 10. a); Monthly (1980-2000) simulated (NCC) aquatic CO₂ evasion vs simulated
 690 discharge on the Madeira River at Porto Velho and b); Observed aquatic CO₂ evasion vs
 691 observed on the Madeira River at Porto Velho, measured between 2009 and 2011.

692
 693 The pattern of interannual variation in NEP over the 1980s and 1990s in our results is
 694 consistent with that found in previous modelling studies over the same period (Prentice and
 695 Lloyd, 1998; Tian et al., 1998). Interestingly we find smaller interannual variation than these
 696 previous modelling studies that did not include inland water fluxes, further supporting the
 697 idea that incorporating aquatic fluxes dampens the interannual variation in NEP. Indeed, a
 698 2013 study (Wang et al., 2013) found results to suggest that some DGVMs overestimate the
 699 sensitivity of net ecosystem exchange (NEE) to precipitation. The relationship between our
 700 simulated NEP and precipitation is generally weaker than that found in previous models
 701 across the tropical region (Wang et al., 2013, in this case NEE), and the addition of the

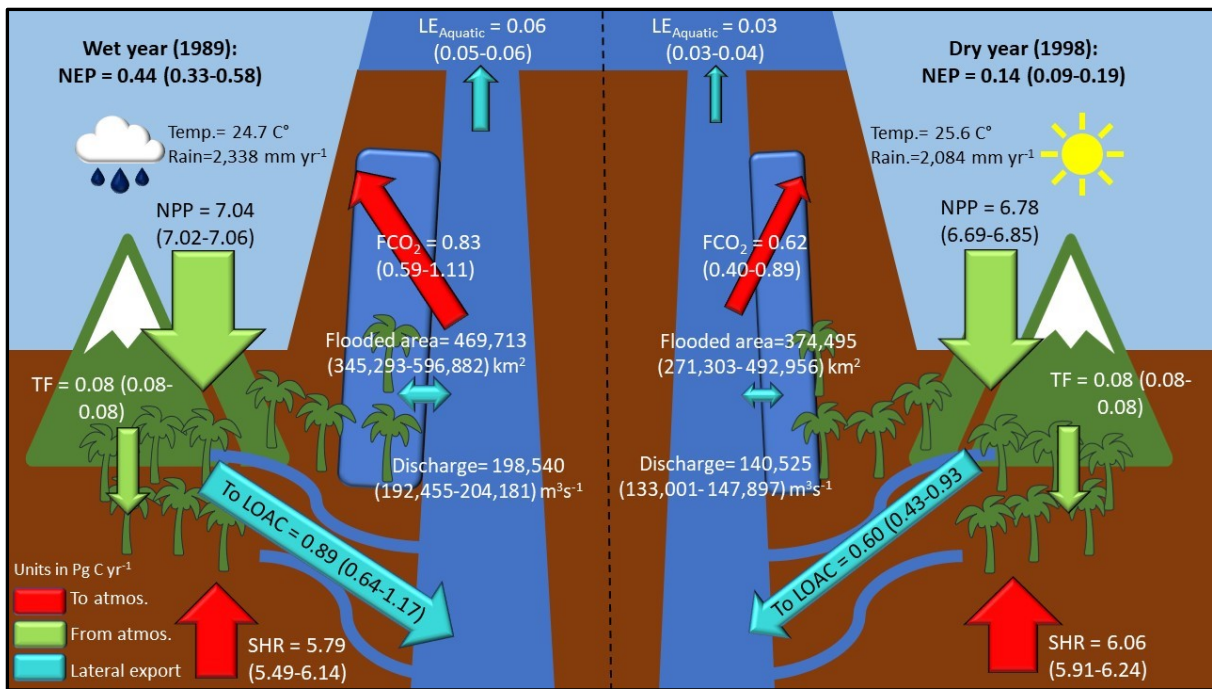
702 aquatic C fluxes appears to be at least partly responsible for this; the sum of terrestrial fluxes
703 (NPP-SHR) is more strongly correlated with precipitation (detrended $R^2 = 0.58$, $p < 0.0001$
704 NCC run; detrended $R^2 = 0.51$, $p < 0.0001$ with Princeton GPCC run) than NEP (detrended R^2
705 $= 0.27$, $p < 0.05$ NCC run; detrended $R^2 = 0.25$, $p < 0.01$ with Princeton GPCC run), which
706 includes aquatic components.

707 Despite some of the limitations of DGVMs discussed, namely their inability to fully capture
708 the complex effects of droughts on NPP, the response of our model to drought events concurs
709 with observational based studies, and most significantly to those based on the measurement
710 of atmospheric CO_2 fluxes. The 2010 Amazon drought was one of the most severe ever
711 recorded and related to another El Nino event, as well as anomalous SSTs (Lewis et al.,
712 2011). Gatti et al. (2014) used small aircraft to measure CO_2 fluxes just above the Amazon
713 rainforest (lower-troposphere) and found that in 2010, the Amazon basin was a net source to
714 the atmosphere of $0.48 \pm 0.18 \text{ Pg C yr}^{-1}$. A 2015 study (van der Laan-Luijkx et al., 2015),
715 further constrained the results of Gatti et al. using remote sensing data and estimated a
716 smaller atmospheric CO_2 source between 0.07 and $0.31 \text{ Pg C yr}^{-1}$ for 2010. Based on our
717 Princeton GPCC run, we similarly estimate that in 2010, the Amazon was an overall CO_2
718 source for the atmosphere of 0.33 ($0.35 - 0.29$) Pg C yr^{-1} (based on NBP). Additionally, using
719 a combined remote sensing and modelling approach, Potter et al. (2011) estimated that the
720 2010 drought caused a loss of biomass in the Amazon of 0.5 Pg C yr^{-1} relative to the strong
721 La Nina year of 2008, and we produce a similar NEP deficit $0.51 \text{ Pg C yr}^{-1}$.

722 In Figure 11, we show our simulated C budget for a drought year, 1998, and an anomalously
723 wet year, 1989, to illustrate how both terrestrial and aquatic C fluxes react to climatic
724 extremes. In 1989, high aquatic CO_2 evasion to the atmosphere driven by high rainfall and
725 large floodplain inundation, partly offsets a relatively large terrestrial sink, caused by high
726 terrestrial NPP and low SHR. In 1998 the opposite occurs; low rainfall results in a low flux of

727 CO₂ from inland waters to the atmosphere, which moderates a relatively high SHR flux and
728 low terrestrial NPP. As previously noted, aquatic CO₂ evasion is highly sensitive to rainfall
729 and in turn both discharge and inundation, and displays greater interannual variation than the
730 terrestrial C fluxes. Aquatic CO₂ evasion is positively correlated with NPP but the two fluxes
731 represent opposite signals in terms of C exchange with the atmosphere, while aquatic CO₂
732 evasion is inversely correlated to SHR, both fluxes being C sources for the atmosphere. For
733 these two reasons, the aquatic fluxes generally act to compensate the difference between
734 terrestrial NPP and SHR and thus dampen overall interannual variation in the net C balance.

735 Another process not accounted for in our model is C sequestration on floodplains.
736 Interestingly, a 2003 study (Aalto et al., 2003) showed that, sediment accumulation on
737 Amazon floodplains is closely linked to the ENSO cycle. Like our findings for aquatic CO₂
738 evasion, sediment accumulation was found to be higher during La Nina years, and most
739 notably in 1988. Despite not accounting for this C sink term in our model, the comparison of
740 our net C balance for the Amazon (NBP) against observations (Grace et al., 2016) suggests
741 that if anything we are still underestimating the net flux of C from the Amazon basin to the
742 atmosphere.



743

744 Figure 11. Simulated annual C budget for left; the Amazon basin for the year 1989, and right;
 745 the Amazon basin for the year 1998, where NEP is net ecosystem production, NPP is
 746 terrestrial net primary productivity, TF is throughfall, SHR is soil heterotrophic respiration,
 747 FCO_2 is aquatic CO_2 evasion, LOAC is C leakage to the land-ocean aquatic continuum
 748 (FCO_2 + to coast), and $LE_{Aquatic}$ is the export C flux to the coast. Numbers refer to mean
 749 across the six simulations while numbers in parentheses refer to range.

750 4.2 The importance of integrating the LOAC within the land carbon cycle

751 The Amazon is facing a number of threats including climate change, land use change and
 752 dam construction (Nobre et al., 2016). Climatic events such as droughts and floods are
 753 becoming more frequent (Marengo et al., 2011; Gloor et al., 2013; Zulkafli et al., 2016),
 754 while southern Amazonia has experienced a general lengthening of the dry season (Fu et al.,
 755 2013). The region is also undergoing a boom in dam construction with 140 dams under
 756 construction or already in operation, and a further 288 planned (Latrubesse et al., 2017) with
 757 direct impact on the C retention efficiency within the LOAC (Maavara et al., 2017). In
 758 addition, a recent study demonstrated that the lowland floodplain forests of the Amazon are
 759 less resilient to fires than terra firme forests (Flores et al., 2017).

760 For these reasons, it is vital that the flood dynamics of the Amazon can be correctly
761 represented in biogeochemical models. The implementation of a new floodplain forcing file
762 based on high resolution SAR data substantially improves our ability to accurately simulate
763 the seasonality in observed flooding. Moreover, it leads to a 97% increase in our estimate of
764 mean annual CO₂ evasion from the river-floodplain aquatic continuum and supports some
765 larger previous estimates based on simple upscaling approaches (Table S4). Our results show
766 that the LOAC fluxes, highly sensitive to hydrological variation, display greater interannual
767 variation than the terrestrial C fluxes (NPP – SHR), and are thus disproportionately important
768 to the overall variation of the net C balance, relative to their magnitude. We also find that the
769 percentage of NPP lost to the LOAC is variable at the interannual timescale (Fig. 11).

770 Our results suggest that the linkage between the terrestrial and aquatic environment may be
771 larger than previously thought and our estimate of aquatic CO₂ evasion from the Amazon is
772 of a globally significant magnitude in terms of aquatic C fluxes. However, these results must
773 be placed within the context of their overall impact on the net C balance of the Amazon
774 Basin. While greater inundation increases aquatic CO₂ evasion, it simultaneously decreases
775 the decomposition of organic matter in litter and soils and we show that the net impact of
776 greater flooding is in fact a reduction in the flux of CO₂ from the Amazon basin to the
777 atmosphere. It is during years with the lowest precipitation, often associated with El Nino
778 events that highest net flux of CO₂ to the atmosphere are simulated. Indeed, we find that
779 aquatic C fluxes partly compensate terrestrial C fluxes, and therefore moderate the overall
780 interannual variation in NEP. Thus, DGVMs that do not account for aquatic fluxes may
781 overestimate the magnitude of interannual variation in NEP. This calls for a fully integrated
782 view of the land carbon cycle, which cannot be achieved with empirical studies alone and
783 highlights the value of a model that can integrate the terrestrial and aquatic C cycles.

784

785

786

787

788

789 **Acknowledgments**

790 Financial support was received from the European Union’s Horizon 2020 research and
791 innovation program under the Marie Skłodowska- Curie grant agreement No. 643052 (C-
792 CASCADES project). RL acknowledges funding from the European Union’s Horizon 2020
793 research and innovation program under grant agreement no. 703813 for the Marie
794 Skłodowska-Curie European Individual Fellowship “C-Leak.” PR acknowledges funding
795 from the Belgian Federal Science Policy Office (BELSPO), project “Global impacts of
796 hydrological and climatic extremes on vegetation” (SAT-EX) – Belgian research programme
797 for Earth Observation Stereo III.

798

799

800

801

802

803

804

805

806

807

808

809 **References**

- 810 Aalto, R., L. Maurice-Bourgoin, T. Dunne, D. R. Montgomery, C. A. Nittrouer, and J. L.
811 Guyot (2003), Episodic sediment accumulation on Amazonian flood plains influenced
812 by El Nino/Southern Oscillation, *Nature*, 425, 493–497, doi:10.1038/nature02002
- 813 Abril, G., Martinez, J.-M., Artigas, L. F., Moreira-Turcq, P., Benedetti, M. F., Vidal, L., ...
814 Roland, F. (2013). Amazon River carbon dioxide outgassing fuelled by wetlands.
815 *Nature*, 505, 395. Retrieved from <http://dx.doi.org/10.1038/nature12797>
- 816 Abril, G. and Borges, A. V.: Carbon leaks from flooded land: do we need to re-plumb the
817 inland water active pipe?, *Biogeosciences Discuss.*, [https://doi.org/10.5194/bg-2018-](https://doi.org/10.5194/bg-2018-239)
818 239, in review, 2018.
- 819 Ahlström, A., Raupach, M. R., Schurgers, G., Smith, B., Arneeth, A., Jung, M., ... Zeng, N.
820 (2015). The dominant role of semi-arid ecosystems in the trend and variability of the
821 land CO₂ sink. *Science*, 348(6237), 895-899. DOI: 10.1126/science.aaa1668
- 822 Andreoli, R. V., Ferreira de Souza, R. A., Kayano, M. T. and Candido, L. A. (2012),
823 Seasonal anomalous rainfall in the central and eastern Amazon and associated
824 anomalous oceanic and atmospheric patterns. *Int. J. Climatol.*, 32: 1193-1205.
825 doi:[10.1002/joc.2345](https://doi.org/10.1002/joc.2345)
- 826 Almeida, R. M., Pacheco, F. S., Barros, N., Rosi, E., & Roland, F. (2017). Extreme floods
827 increase CO₂ outgassing from a large Amazonian river. *Limnology and Oceanography*,
828 62(3), 989–999. <https://doi.org/10.1002/lno.10480>
- 829 Asner, G. P., Townsend, A. R., & Braswell, B. H. (2000). Satellite observation of El Niño
830 effects on Amazon Forest phenology and productivity. *Geophysical Research Letters*,
831 27(7), 981–984. <https://doi.org/10.1029/1999GL011113>
- 832 Aufdenkampe, A. K., Mayorga, E., Raymond, P. A., Melack, J. M., Doney, S. C., Alin, S. R.,
833 ... Yoo, K. (2011). Riverine coupling of biogeochemical cycles between land, oceans,
834 and atmosphere. *Frontiers in Ecology and the Environment*, 9(1), 53–60.
835 <https://doi.org/10.1890/100014>
- 836 Battin, T. J., Luysaert, S., Kaplan, L. A., Aufdenkampe, A. K., Richter, A., & Tranvik, L. J.
837 (2009). The boundless carbon cycle. *Nature Geoscience*, 2, 598. Retrieved from
838 <https://doi.org/10.1038/ngeo618>
- 839 Bond-Lamberty, B.P. and A.M. Thomson. 2014. A Global Database of Soil Respiration Data,
840 Version 3.0. Data set. Available on-line [<http://daac.ornl.gov>] from Oak Ridge National
841 Laboratory Distributed Active Archive Center, Oak Ridge, Tennessee,
842 USA. <http://dx.doi.org/10.3334/ORNLDAAAC/1235>
- 843 Botta, A., Ramankutty, N., & Foley, J. A. (2002). Long-term variations of climate and carbon
844 fluxes over the Amazon basin. *Geophysical Research Letters*, 29(9), 33–34.
845 <https://doi.org/10.1029/2001GL013607>

- 846 Camino-Serrano, M., Guenet, B., Luyssaert, S., Janssens, I.A., 2018. ORCHIDEE-SOM:
847 modeling soil organic carbon (SOC) and dissolved organic carbon (DOC) dynamics
848 along vertical soil profiles in Europe. *Geosci. Model Dev.* 11, 937–957
- 849 Chou, C., Chiang, J. C. H., Lan, C.-W., Chung, C.-H., Liao, Y.-C., & Lee, C.-J. (2013).
850 Increase in the range between wet and dry season precipitation. *Nature Geoscience*, 6,
851 263. Retrieved from <http://dx.doi.org/10.1038/ngeo1744>
- 852 Ciais, P., Sabine, C., Bala, G., Bopp, L., Brovkin, V., Canadell, J., . . . (2013). Carbon and
853 Other Biogeochemical Cycles. In T. F. Stocker, D. Qin, G.-K. Plattner, M. Tignor, S. K.
854 Allen, J. Boschung, A. Nauels, Y. Xia, V. Bex, and P. M. Midgley (Eds.), *Climate*
855 *change 2013: The physical science basis. Contribution of working group I to the fifth*
856 *assessment report of the intergovernmental panel on climate change* (pp. 465–570).
857 Cambridge University Press, Cambridge.
- 858 Ciais, P., Gasser, T., Lauerwald, R., Peng, S., Raymond, P. A., Wang, Y., Zhu, D. (2017).
859 Observed regional carbon budgets imply reduced soil heterotrophic respiration. *Nature*,
860 in review.
- 861 Cochonneau, G., Sondag, F., Guyot, J.-L., Geraldo, B., Filizola, N., Fraizy, P., Laraque, A.,
862 Magat, P., Martinez, J.-M., Noriega, L., Oliveira, E., Ordonez, J., Pombosa, R., Seyler,
863 F., Sidgwick, J., and Vauchel, P.: The environmental observation and research project,
864 ORE HYBAM, and the rivers of the Amazon basin, in: *Climate Variability and Change*
865 *– Hydrological Impacts*, IAHS Publ. 308, edited by: Demuth, S., Gustard, A., Planos, E.,
866 Scatena, F., and Servat, E., IAHS Press, UK, 44–50, 2006
- 867 Cole, J. J., Prairie, Y. T., Caraco, N. F., McDowell, W. H., Tranvik, L. J., Striegl, R. G., &
868 Melack, J. (2007). Plumbing the global carbon cycle: Integrating inland waters into the
869 terrestrial carbon budget. *Ecosystems*, 10(1), 172–185. [https://doi.org/10.1007/s10021-](https://doi.org/10.1007/s10021-006-9013-8)
870 [006-9013-8](https://doi.org/10.1007/s10021-006-9013-8)
- 871
872 de Rosnay, P., Polcher, J., Bruen, M., and Laval, K.: Impact of a physically based soil water
873 flow and soil-plant interaction representation for modeling large-scale land surface
874 processes, *J. Geophys. Res.-Atmos.*, 107, ACL3-1–ACL3-19,
875 <https://doi.org/10.1029/2001JD000634>, 2002.
- 876
877 Doughty, C. E., Metcalfe, D. B., Girardin, C. A. J., Amézquita, F. F., Cabrera, D. G., Huasco,
878 W. H., . . . Malhi, Y. (2015). Drought impact on forest carbon dynamics and fluxes in
879 Amazonia. *Nature*, 519, 78. Retrieved from <https://doi.org/10.1038/nature14213>
- 880
881
882 Dos Santos, A., & Nelson, B. (2013). Leaf decomposition and fine fuels in floodplain forests
883 of the Rio Negro in the Brazilian Amazon. *Journal of Tropical Ecology*, 29(5), 455-
884 458. doi:10.1017/S0266467413000485
- 885
886 d’Orgeval, T., Polcher, J., and de Rosnay, P.: Sensitivity of the West African hydrological
887 cycle in ORCHIDEE to infiltration processes, *Hydrol. Earth Syst. Sci.*, 12, 1387–1401,
888 <https://doi.org/10.5194/hess-12-1387-2008>, 2008.
- 889

- 890 Drake, T. W., Raymond, P. A. and Spencer, R. G. (2018), Terrestrial carbon inputs to inland
891 waters: A current synthesis of estimates and uncertainty. *Limnol. Oceanogr.*, 3: 132-
892 142. doi:[10.1002/lol2.10055](https://doi.org/10.1002/lol2.10055)
- 893 Fasullo, J. T., Otto-Bliesner, B. L., & Stevenson, S. (2018). ENSO's Changing Influence on
894 Temperature, Precipitation, and Wildfire In a Warming Climate. *Geophysical Research*
895 *Letters*, 0(ja). <https://doi.org/10.1029/2018GL079022>
- 896 Feldpausch. T., L., P. O., W., B. R. J., E., G., J., L., G., L., ... A., V. V. (2016). Amazon
897 forest response to repeated droughts. *Global Biogeochemical Cycles*, 30(7), 964–982.
898 <https://doi.org/10.1002/2015GB005133>
- 899 Foley, J. A., A. Botta, M. T. Coe, and M. H. Costa, El Niño–Southern oscillation and the
900 climate, ecosystems and rivers of Amazonia, *Global Biogeochem. Cycles*, 16(4), 1132,
901 doi: 10.1029/2002GB001872, 2002.
- 902 Fu, R., Yin, L., Li, W., Arias, P. A., Dickinson, R. E., Huang, L., ... Myneni, R. B. (2013).
903 Increased dry-season length over southern Amazonia in recent decades and its
904 implication for future climate projection. *Proceedings of the National Academy of*
905 *Sciences*, 110(45), 18110–18115. <https://doi.org/10.1073/pnas.1302584110>
- 906 Gatti, L. V., Gloor, M., Miller, J. B., Doughty, C. E., Malhi, Y., Domingues, L. G., ... Lloyd,
907 J. (2014). Drought sensitivity of Amazonian carbon balance revealed by atmospheric
908 measurements. *Nature*, 506, 76. Retrieved from <http://dx.doi.org/10.1038/nature12957>
- 909 Gloor, M. *et al.* The carbon balance of South America: a review of the status, decadal trends
910 and main determinants. *Biogeosciences* 9, 5407–5430 (2012)
- 911 Gloor, M., R. J. W. Brienen, D. Galbraith, T. R. Feldpausch, J. Schöngart, J.-L. Guyot, J. C.
912 Espinoza, J. Lloyd, and O. L. Phillips (2013), Intensification of the Amazon
913 hydrological cycle over the last two decades, *Geophys. Res. Lett.*, 40, 1729–1733,
914 doi: 10.1002/grl.50377.
- 915 Gloor, M., J. Barichivich, G. Ziv, R. Brienen, J. Schöngart, P. Peylin, B. B. Ladvocat
916 Cintra, T. Feldpausch, O. Phillips, and J. Baker (2015), Recent Amazon climate as
917 background for possible ongoing and future changes of Amazon humid forests, *Global*
918 *Biogeochem. Cycles*, 29, 1384–1399, doi:10.1002/2014GB005080.
- 919 Grace J. (2016) The Amazon Carbon Balance: An Evaluation of Methods and Results. In:
920 Nagy L., Forsberg B., Artaxo P. (eds) Interactions Between Biosphere, Atmosphere and
921 Human Land Use in the Amazon Basin. Ecological Studies (Analysis and Synthesis),
922 vol 227. Springer, Berlin, Heidelberg
- 923 Guimberteau, M., Drapeau, G., Ronchail, J., Sultan, B., Polcher, J., Martinez, J.-M., ...
924 Vauchel, P. (2012). Discharge simulation in the sub-basins of the Amazon using
925 ORCHIDEE forced by new datasets. *Hydrology and Earth System Sciences*, 16(3),
926 911–935. <https://doi.org/10.5194/hess-16-911-2012>
- 927 Gumbrecht, T., Roman-Cuesta, R. M., Verchot, L., Herold, M., Wittmann, F., Householder,
928 E., Murdiyarso, D. (2017). An expert system model for mapping tropical wetlands and

- 929 peatlands reveals South America as the largest contributor. *Global Change Biology*,
930 23(9), 3581–3599. <https://doi.org/10.1111/gcb.13689>
- 931 Hastie, A., Lauerwald, R., Weyhenmeyer, G., Sobek, S., Verpoorter, C., Regnier, P (2017).
932 CO2 evasion from boreal lakes: Revised estimate, drivers of spatial variability, and
933 future projections. *Global Change Biology*, 24(2), 711–728.
934 <https://doi.org/10.1111/gcb.13902>
- 935 Hess, L. L., Melack, J. M., Novo, E. M. L. M., Barbosa, C. C. F., and Gastil, M.: Dual-season
936 mapping of wetland inundation and vegetation for the central Amazon basin, *Remote*
937 *Sens. Environ.*, 87, 404–428, 2003
- 938 HESS, L. L., MELACK, J. M., NOVO, E. M. L. M., BARBOSA, C. C. F., & GASTIL, M.
939 (2015). LBA-ECO LC-07 JERS-1 SAR Flooded Wetlands and Vegetation, Amazon
940 Basin: 1995-1996. ORNL Distributed Active Archive Center.
941 <https://doi.org/10.3334/ornldaac/1284>
- 942 Kim, H. (2017). *Global Soil Wetness Project Phase 3 Atmospheric Boundary Conditions*
943 *(Experiment 1)* [Data set]. Data Integration and Analysis System (DIAS).
944 <https://doi.org/10.20783/DIAS.501>
- 945 Latrubesse, E. M., Arima, E. Y., Dunne, T., Park, E., Baker, V. R., d’Horta, F. M., ...
946 Stevaux, J. C. (2017). Damming the rivers of the Amazon basin. *Nature*, 546, 363.
947 Retrieved from <http://dx.doi.org/10.1038/nature22333>
- 948 Lauerwald, R., Laruelle, G. G., Hartmann, J., Ciais, P., & Regnier, P. A. G. (2015). Spatial
949 patterns in CO2 evasion from the global river network. *Global Biogeochemical Cycles*,
950 29(5), 534–554. <https://doi.org/10.1002/2014GB004941>
- 951 Lauerwald, R., Regnier, P., Camino-Serrano, M., Guenet, B., Guimberteau, M., Ducharne,
952 A., ... Ciais, P. (2017). ORCHILEAK (revision 3875): a new model branch to simulate
953 carbon transfers along the terrestrial–aquatic continuum of the Amazon basin.
954 *Geoscientific Model Development*, 10(10), 3821–3859. [https://doi.org/10.5194/gmd-10-](https://doi.org/10.5194/gmd-10-3821-2017)
955 [3821-2017](https://doi.org/10.5194/gmd-10-3821-2017)
- 956 Lehner, B. and Döll, P.: Development and validation of a global database of lakes, reservoirs
957 and wetlands, *J. Hydrol.*, 296, 1–22, <https://doi.org/10.1016/j.jhydrol.2004.03.028>, 2004.
- 958 Lewis, S. L., Brando, P. M., Phillips, O. L., van der Heijden, G. M. F. & Nepstad, D. he 2010
959 Amazon drought. *Science* 331, 554–554 (2011).
- 960 Li, W., Zhang, P., Ye, J., Li, L., & Baker, P. A. (2011). Impact of two different types of El
961 Niño events on the Amazon climate and ecosystem productivity. *Journal of Plant*
962 *Ecology*, 4(1–2), 91–99. Retrieved from <http://dx.doi.org/10.1093/jpe/rtq039>
- 963 Marengo, J. A., J. Tomasella, L. M. Alves, W. R. Soares, and D. A. Rodriguez (2011), The
964 drought of 2010 in the context of historical droughts in the Amazon region, *Geophys.*
965 *Res. Lett.*, 38, L12703, doi:10.1029/2011GL047436.

- 966 Maavara, T., Lauerwald, R., Regnier, P., & Van Cappellen, P. (2017). Global perturbation of
967 organic carbon cycling by river damming, *8*, 15347. Retrieved from
968 <http://dx.doi.org/10.1038/ncomms15347>
- 969 Medlyn, B. E. (2011). Comment on {\textquotedblleft}Drought-Induced Reduction in Global
970 Terrestrial Net Primary Production from 2000 Through 2009{\textquotedblright}.
971 *Science*, *333*(6046), 1093. <https://doi.org/10.1126/science.1199544>
- 972 Melack, J.M., L.L. Hess, M. Gastil-Buhl, B.R. Forsberg, S.K. Hamilton, I.B.T. Lima, and
973 E.M.L.M. Novo. 2011. LBA-ECO LC-07 Monthly Mean Flooded Wetlands Habitat,
974 Central Amazon Basin: 1979-1996. ORNL DAAC, Oak Ridge, Tennessee, USA.
975 <https://doi.org/10.3334/ORNLDAAC/1049>
- 976 Moreira-Turcq, P., Seyler, P., Guyot, J. L., & Etcheber, H. (2003). Exportation of organic
977 carbon from the Amazon River and its main tributaries. *Hydrological Processes*, *17*(7),
978 1329–1344. <https://doi.org/10.1002/hyp.1287>
- 979 Nemani, R.R., et al., 2003: Climate-driven increases in global terrestrial net primary
980 production from 1982 to 1999. *Science*, *300*, 1560–1563.
- 981 Ngo-Duc, T., Polcher, J., and Laval, K (2005).: A 53-year forcing data set for land surface
982 models, *J. Geophys. Res.-Atmos.*, *110*, D06116, <https://doi.org/10.1029/2004JD005434>
- 983 Nobre, C. A., Sampaio, G., Borma, L. S., Castilla-Rubio, J. C., Silva, J. S., & Cardoso, M.
984 (2016). Land-use and climate change risks in the Amazon and the need of a novel
985 sustainable development paradigm. *Proceedings of the National Academy of Sciences*,
986 *113*(39), 10759–10768. <https://doi.org/10.1073/pnas.1605516113>
- 987 Pangala, S. R., Enrich-Prast, A., Basso, L. S., Peixoto, R. B., Bastviken, D., Hornibrook, E.
988 R. C., ... Gauci, V. (2017). Large emissions from floodplain trees close the Amazon
989 methane budget. *Nature*, *552*, 230. Retrieved from <https://doi.org/10.1038/nature24639>
- 990 Phillips, O. L., Aragão, L. E. O. C., Lewis, S. L., Fisher, J. B., Lloyd, J., López-González, G.,
991 ... Torres-Lezama, A. (2009). Drought Sensitivity of the Amazon Rainforest. *Science*,
992 *323*(5919), 1344–1347. <https://doi.org/10.1126/science.1164033>
- 993 Potter, C., S. Klooster, C. Hiatt, V. Genovese, and J. C. Castilla-Rubio (2011), Changes in the
994 carbon cycle of the Amazon ecosystem during the 2010 drought, *Environ. Res. Lett.*, *6*,
995 [doi:10.1088/1748-9326/6/3/034024](https://doi.org/10.1088/1748-9326/6/3/034024).
- 996 Prentice, I., and J. Lloyd. 1998. C-quest in the Amazon Basin. *Nature* *396*:619–620.
- 997 R Core Team. (2013). R: A language and environment for statistical computing. [Available at
998 <http://www.r-project.org>.]
- 999 Rasera, M. F. F. L., Krusche, A. V., Richey, J. E., Ballester, M. V. R., and Victória, R. L.
1000 (2013). Spatial and temporal variability of pCO₂ and CO₂ efflux in seven Amazonian
1001 Rivers. *Biogeochemistry*, *116*(1), 241–259. <https://doi.org/10.1007/s10533-013-9854-0>

- 1002 Regnier, P., Friedlingstein, P., Ciais, P., Mackenzie, F. T., Gruber, N., Janssens, I. A., ...
1003 Thullner, M. (2013). Anthropogenic perturbation of the carbon fluxes from land to
1004 ocean. *Nature Geosci*, 6(8), 597–607. Retrieved from
1005 <http://dx.doi.org/10.1038/ngeo1830>
- 1006 Resplandy, L., Keeling, R. F., Rödenbeck, C., Stephens, B. B., Khatiwala, S., Rodgers, K. B.,
1007 ... Tans, P. P. (2018). Revision of global carbon fluxes based on a reassessment of
1008 oceanic and riverine carbon transport. *Nature Geoscience*, 11(7), 504–509.
1009 <https://doi.org/10.1038/s41561-018-0151-3>
- 1010 Richey Jeffrey E. , Hedges John I. , Devol Allan H. , Quay Paul D. , Victoria Reynaldo ,
1011 Martinelli Luiz , Forsberg Bruce R. , (1990), Biogeochemistry of carbon in the Amazon
1012 River, *Limnology and Oceanography*, 35, doi: 10.4319/lo.1990.35.2.0352.
- 1013 Richey, J. E., Melack, J. M., Aufdenkampe, A. K., Ballester, V. M., & Hess, L. L. (2002).
1014 Outgassing from Amazonian rivers and wetlands as a large tropical source of
1015 atmospheric CO₂. *Nature*, 416, 617. Retrieved from <http://dx.doi.org/10.1038/416617a>
- 1016 Richey, J.E., R.L. Victoria, J.I. Hedges, T. Dunne, L.A. Martinelli, L. Mertes, and J. Adams.
1017 2008. Pre-LBA Carbon in the Amazon River Experiment (CAMREX) Data. ORNL
1018 DAAC, Oak Ridge, Tennessee, USA. <https://doi.org/10.3334/ORNLDAAAC/904>
- 1019 Rödig E, Cuntz M, Rammig A, Fischer R, Taubert F and Huth A. (2018). The importance of
1020 forest structure for carbon fluxes of the Amazon rainforest. *Environmental Research*
1021 *Letters*, 13(5), 54013. Retrieved from <http://stacks.iop.org/1748-9326/13/i=5/a=054013>
- 1022 Rueda-Delgado, G., Wantzen, K. M., and Tolosa, M. B.: Leaf litter decomposition in an
1023 Amazonian floodplain stream: Effects of seasonal hydrological changes, *J. North Am.*
1024 *Benthol. Soc.*, 25, 233–249, <https://doi.org/10.1899/0887>
1025 3593(2006)25[233:LDIAAF]2.0.CO;2, 2006.
- 1026 Sanders, L. M., Taffs, K. H., Stokes, D. J., Sanders, C. J., Smoak, J. M., Enrich-Prast, A. ,
1027 Macklin, P. A., Santos, I. R. and Marotta, H. (2017), Carbon accumulation in
1028 Amazonian floodplain lakes: A significant component of Amazon budgets?. *Limnol.*
1029 *Oceanogr.*, 2: 29-35. doi:[10.1002/lo2.10034](https://doi.org/10.1002/lo2.10034)
- 1030 Sheffield, J., Goteti, G., & Wood, E. F. (2006). Development of a 50-Year High-Resolution
1031 Global Dataset of Meteorological Forcings for Land Surface Modeling. *Journal of*
1032 *Climate*, 19(13), 3088–3111. <https://doi.org/10.1175/JCLI3790.1>
- 1033 Tian, H., J. M. Melillo, D. W. Kicklighter, A. D. McGuire, J. V. K. Helfrich, B. Moore, and
1034 C. J. Vorosmarty. 1998. Effect of interannual climate variability on carbon storage in
1035 Amazonian ecosystems. *Nature* 396:664–667.
- 1036 Tranvik, L. J., Downing, J. A., Cotner, J. B., Loiselle, S. A., Striegl, R. G., Ballatore, T. J., . .
1037 . Weyhenmeyer, G. A. (2009). Lakes and reservoirs as regulators of carbon cycling and
1038 climate. *Limnology and Oceanography*, 54(6 part 2), 2298–2314.
1039 https://doi.org/10.4319/lo.2009.54.6_part_2.2298

- 1040 van der Laan-Luijkx, I. T., I. R. van der Velde, M. C. Krol, L. V. Gatti, L. G. Domingues, C.
1041 S. C. Correia, J. B. Miller, M. Gloor, T. T. van Leeuwen, J. W. Kaiser, et al.
1042 (2015), Response of the Amazon carbon balance to the 2010 drought derived with
1043 CarbonTracker South America, *Global Biogeochem. Cycles*, 29, 1092–1108,
1044 doi: 10.1002/2014GB005082.
- 1045 Vörösmarty, C. J., Fekete, B. M., Meybeck, M., and Lammers, R. B.: Geomorphometric
1046 attributes of the global system of rivers at 30-minute spatial resolution, *J. Hydrol.*, 237,
1047 17–39, 2000.
- 1048 Wang, W., Ciais, P., Nemani, R. R., Canadell, J. G., Piao, S., Sitch, S., White, M. A.,
1049 Hashimoto, H., Milesi, C., and Myneni, R. B.: Variations in atmospheric CO₂ growth
1050 rates coupled with tropical temperature, *Proc. Natl. Acad. Sci. USA*, 110, 13061–13066,
1051 doi:10.1073/pnas.1219683110, 2013.
- 1052 Wolter, K., and M. S. Timlin, 2011: El Niño/Southern Oscillation behaviour since 1871 as
1053 diagnosed in an extended multivariate ENSO index (MEI.ext). *Intl. J. Climatology*, **31**,
1054 14pp., 1074-1087
- 1055 Zarfl, C., Lumsdon, A. E., Berlekamp, J., Tydecks, L., & Tockner, K. (2015). A global boom
1056 in hydropower dam construction. *Aquatic Sciences*, 77(1), 161–170.
1057 <https://doi.org/10.1007/s00027-014-0377-0>
- 1058 Zhao, M., & Running, S. W. (2010). Drought-Induced Reduction in Global Terrestrial Net
1059 Primary Production from 2000 Through 2009. *Science*, 329(5994), 940–943.
1060 <https://doi.org/10.1126/science.1192666>
- 1061 Zulkafli, Z., Buytaert, W., Manz, B., Rosas, C. V., Willems, P., Lavado-Casimiro, W., Guyot,
1062 J.-L., and Santini, W.: Projected increases in the annual flood pulse of the Western
1063 Amazon, *Environ. Res. Lett.*, 11, 14013, doi:10.1088/1748-9326/11/1/014013, 2016.
- 1064
- 1065
- 1066